12-8-2015

Design of a Tandem Rotor Hovering Vehicle

Brent Kostich
Western Michigan University, bkostich@icloud.com

Western Michigan University

Department of Mechanical and Aerospace Engineering

Advised by: Dr. Kapseong Ro

Design of a Tandem Rotor Hovering Vehicle

Project Number #12 - 15 - 4

Steven Beuerle

Brent Kostich

Nicole St. Louis

Andrew Verstraete

DISCLAIMER

This project report was written by students at Western Michigan University to fulfill an engineering curriculum requirement. Western Michigan University makes no representation that the material contained in this report is error-free or complete in all respects. Persons or organizations who choose to use this material do so at their own risk.

Abstract

An investigation of thrust vectoring and an examination of existing tandem rotor dynamics were used to develop a structural body for a tandem rotor vehicle, derive the equations of motion of the system, and simulate a dynamic model of the vehicle. A vehicle prototype was constructed while further application of remote control capabilities, flight testing, and control development were researched. The dynamic simulation was based on a linear model of the system so as to open the possibility of implementing a control system. The simulation results show that thrust synchronization yields a predictable motion response. The prototype constructed did not have synchronized thrust between the rotors and the simulation results show a divergent response to perturbations from equilibrium. This project can be scaled and applied to recreation vehicles of the future, specifically in the growing area of hover vehicle technology.

Table of Contents

List of Figures

1. Background and Research

This project was motivated by the desire to further the research in the field of modern rotocopter design and implementation. With recent advances in technology, both in terms of hardware and software, the market for personal and commercial use of rotocopter vehicles has rapidly expanded. Therefore, this project's desire was to push the envelope of the less common non-coaxial tandem rotor design to aid in ushering in the current and upcoming market for these vehicles.

One of the primary design issues with tandem rotor vehicles is their lack of multidimensional control inputs. For example, the common quadcopter has four individual motors that allow for control of the roll, pitch, and yaw by merely increasing or decreasing thrust at a given motor. Tandem rotors do not have such a luxury, thus many modern designs make use of advanced mechanical control devices, such as a swashplates, to attain the same level of controllability. A swashplate is a mechanism that allows for cyclic and collective changes of the pitch of a rotor. This allows for vectoring of thrust to establish control in all three directions. [1]

The use of mechanisms like swashplates are quite common in many contemporary applications. Thus, a number of papers covering the topic of tandem rotor dynamics have been found to contain some inclusion of such a device. This situation complicates the dynamics of the vehicles even further. In order to establish an understanding based on first principles, the background research led to the rejection of the swashplate scheme for a simpler one based on single-axis rotation for control input, which is discussed in greater detail further in the report.

A review of literature describing the dynamics of such vehicles yielded the expected results of a classic six degree-of-freedom body. In order to appropriately describe the system, all six degrees must be taken into consideration, in some detail, to develop the equations of motion (EOMs). These dynamic and kinematic equations allow for not only the definition of the system, but also lay the foundation by which numerical simulations would take place. Furthermore, it was understood that many aspects of the governing dynamics of this system are highly nonlinear. A common method is to linearize the EOMs in order to attain more suitable equations for system simulation. Therefore, this approach was implemented, which is discussed to greater extent later in the report. [1]

2. Problem Description

This project's overall goal was to successfully design a tandem rotor vehicle. The idea was built around the concept of having a human pilot a full-scale version, similar to the scaled down model shown in Figure 1, but with only two rotors. Due to the time and money that was available for this project, the goal was to build a tandem rotor vehicle, but at a scaled, remote controlled level. Completion of this project included several components. First was developing a structural body that is able to support the imposed static and dynamic loads. Next, deriving and modeling the dynamic equations of motion to determine the stability and response of the system, followed by simulating the dynamic model within the operational parameters to develop synchronous control of tandem-rotors. Finally, constructing a physical version of the vehicle under the parameters designed in the model and simulation concluded the project.

Figure 1: Similar existing design concept [2]

3. Vehicle Design

A number of things needed to be considered in the design of this vehicle. Due to constraints of time and money, this was not a full-scale model and cannot support a human rider, but rather a scaled model for remote control (RC). Being an RC vehicle, a good deal of research was conducted into the component selection for motors, servos, batteries, and propellers. The proper components had to be selected to be able to produce the necessary thrust to lift the frame and the weight of the components, as well as the weight of any additional control systems to be added in the future. As a tandem rotor vehicle, the orientation of the rotors relative to the direction of forward motion was also a crucial determination. Each orientation option has different pros and cons as far as controllability and complexity. As such, the orientation had to be selected to yield the less expensive and simpler design. All of this said, none of the components and orientation have any bearing unless there is a frame on which they can be applied. Designing an actual physical structure involved material selection as well as deciding on an optimal frame geometry for low complexity and cost, while still maintaining a high enough stiffness to withstand the applied forces of the weight of the system and the lift from the two propellers.

3.1. Frame Design

The final design on the frame was selected based on its simplicity of construction and its ability to meet the structural requirements. The general frame design can be seen in Figure 2.

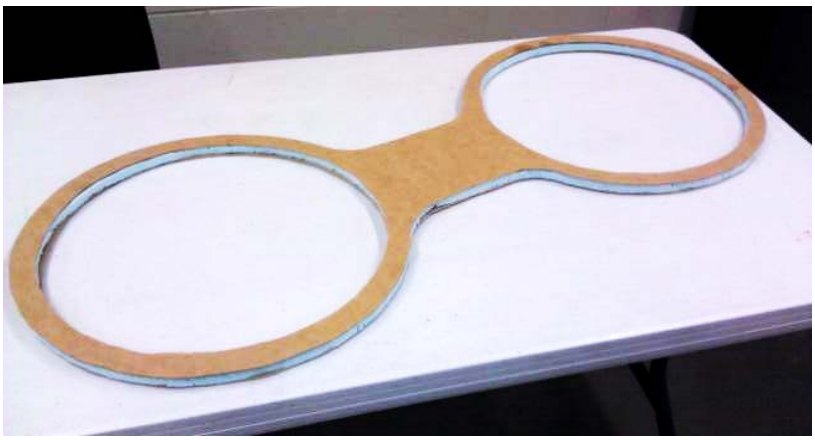

Figure 2: Frame design

Geometrically, the frame is simply composed of two circular sections connected by a rectangular mid-section. The circular sections are where the motors and propellers were mounted, with the intent of the circles being to protect the components in flight, particularly the propellers. The mid rectangular section houses the other components, such as the batteries, electronic speed controllers (ESCs), and the servos. These components were placed in the middle not only for convenience and for wiring purposes, but also so that they will cause less bending stress on the frame by keeping them close to the centroid and minimizing their moment arm.

3.1.1 Material Selection

One aspect of the vehicle design was the material selection for the frame components. The design requirements call for the frame to be light, but stiff. The frames primary source of load would merely be the components attached to it, which are quite light, other than the two batteries. Therefore, the frame does not need to support a great deal of weight. Rigidity was a necessity for several reasons. First, the mathematical model of the vehicle was derived assuming a rigid body, and thus for accuracy the frame needed to match as closely as plausible. Second, from a physical sense, the thrust and weight forces acting on the vehicle tend to bend the frame concave upward. This is highly undesirable for general flight controllability. For reasons that will be further explained later in this section, concavity would yield thrust in an undesired direction. That thrust was not accounted for in the simulated model. Thus, less concavity is better.

While the list of available materials is quite vast, a practical and qualitative approach was taken to narrow down the candidates. This process was facilitated using Ashby charts. Shown in Figure 3 is a classic example of a stiffness versus weight plot, expressed by the material properties of modulus of elasticity and density, E and ρ.[3]

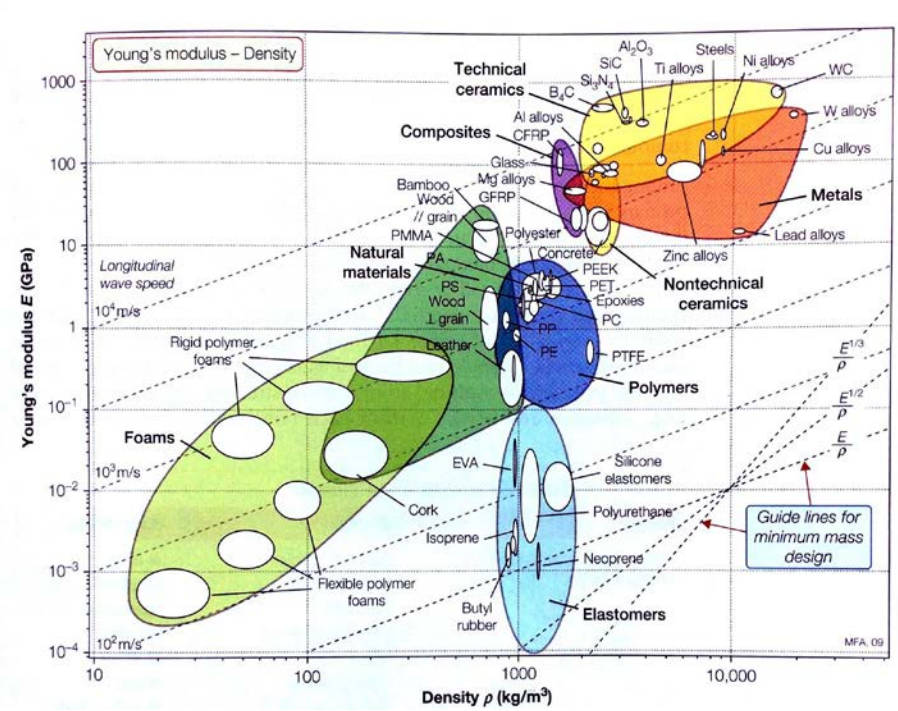

Figure 3: Ashby chart for Young's modulus vs. density [3]

Using the design guidelines, it is clear that the best-suited materials reside in the top right portion of the plot. However, as outlined above, the overall weight of the craft is important, thus another design guideline was included at the density equal to 500 kg/m^3. After this addition, it was clear that the best materials were in the wood and foam regions.

The sandwich core design was used to increase bending stiffness while achieving an overall low density. [4] As shown in Figure 4, in sandwich core structures the outer sheets carry the tensile and compressive bending loads while the core carries the shear load.

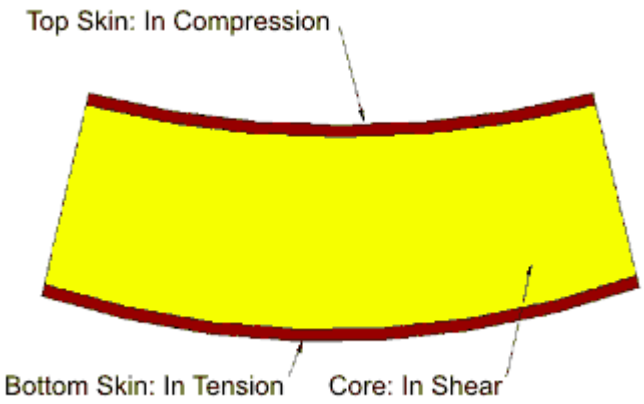

Figure 4: Sandwich structure [4]

The further the two outer sheets are from each other, the stiffer the structure is when subjected to bending loads. This is because the stiffness of a structure in bending directly relates to the area moment of inertia of the cross section. The area moment of inertia, *I*, in a single rectangular element of a composite-shape cross section is as follows:

$$I = \frac{1}{12}bh^3 + Ad^2 \quad (1)$$

Where,

$b =$ *length of the side of the rectangle parallel to the neutral axis*
$h =$ *length of the side of the rectangle perpendicular to the neutral axis*
$A =$ *area of the rectangle*
$d =$ *distance from the center of the rectangle to the neutral axis*

As an example, the moment of inertia for 1/8x6" board on top and bottom without any foam in between would be $7.813 \cdot 10^{-3}$ in^4. Adding only 1" of foam in between the two boards (and assuming that the boards take all of the bending) yields a moment of inertia value of 1.695 in^4. The *I* value increased by a factor of over 200 by just adding an inch of foam. Therefore, 0.5"-1.0" was assumed to be a good core thickness for this project because it allows the foam to give sufficient strength contribution without too much of an overall weight penalty.

Two frames were built and tested for bending stiffness. Both frames were constructed using a sandwich type layout consisting of a foam core between two wooden sheets. Frame 1 used 1/8" hardboard with 3/4" foam while frame 2 utilized 3/16" plywood with 1" foam. In both cases, foam safe caulk was used to apply the two wooden layers to the foam. The hardboard had a density and modulus of elasticity, *E*, of approximately 1.84 slugs·ft^{-3} and 6·10^5 psi respectively. [5] The geometry of this design had a bending stiffness, *EI*, approximately equal to 5.95·10^5 lb·in^2. As for the plywood, the same parameters in the same order as above were 0.97 slugs·ft^{-3}, 1.1·10^6 psi, and 2.97·10^6 lb·in^2. The hardboard was more readily available, less expensive, and faster to manufacture than the plywood and was thus used for initial testing. The hardboard frame proved that the sandwich structure was a good option to hold the loads, so an actual analysis of various materials was conducted. After testing, which is further described in the Testing section of this report, the plywood frame design was selected due to its lower weight and better bending characteristics.

3.2. Orientation

A crucial element of the project is the orientation of the vehicle, i.e. where the rotors lie relative to the direction of motion. Two orientations were considered, and the orientation chosen was forward motion perpendicular to the axis of the rotors. The direction of forward motion was defined along the body x-axis with the rotors aligned in the body y-axis and the body z-axis pointing toward the ground. This orientation can be seen below in Figure 5.

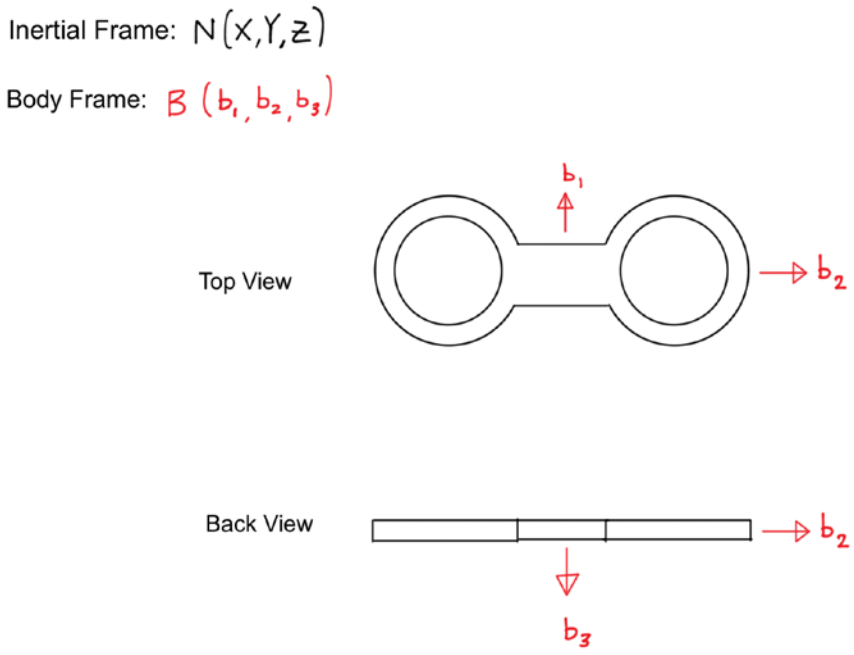

Figure 5: Orientation of vehicle using the body frame axes

The reason this orientation was chosen was in large part due to the non-coaxial nature of the rotors. Hovering, as well as forward flight and turning flight, were all to be controlled via thrust vectoring only, not pitching the frame.

In conjunction with the decision of vehicle orientation, it was also determined that servos would be used for thrust vectoring rather than differential thrust or swashplates. Again, this is largely due to the rotors being non-coaxial. Servos were chosen because they can tilt the rotors equally to vector the thrust while maintaining a consistent angular momentum between the two rotors. Additionally, using differential thrust by increasing the revolutions per minute (RPM) of one rotor to pitch the entire frame to create forward motion also yields a differential angular momentum leading to angular acceleration. Swashplates would maintain RPMs in both rotors, but would also pitch the frame. Also, the complexity, size, and cost of swashplates made them less feasible.

With servos chosen for the thrust vectoring, the rotor orientation was chosen along the y-axis in order to double the usefulness of the servos, compared to an x-axis rotor orientation, while maintaining a simpler frame design. Aligning the servos for y-axis rotations enabled both forward motion and turning motion to be achieved; forward by tilting both rotors in the same direction, and turning by tilting them opposite directions. When a rotor is tilted forward from the

vertical thrust position, the thrust is vectored into the direction of tilt. If the rotors are tilted unequal amounts, or in opposite directions, this vectored thrust in the tilt direction would contribute a moment about the z-axis. This moment is what would provide this frame orientation with the ability to rotate. In the event that both of the rotors are tilted the same amount in the same direction, the moment contribution from the motors cancel each other out and the result is pure thrust in the direction of tilt, yielding translation. If the rotors were to be aligned such that the forward motion were in the same axis as the rotors, the rotors would have to be able to rotate about two axes in order to be able to achieve both forward and turning flight. This is because in tilting the rotors in the direction of desired motion, this orientation would not give a moment about the z-axis because both of the vectored thrusts lie along the body y-axis, acting through the z-axis. In order to turn there would need to be a moment generated about the z-axis, which means that the servos would have to be able to rotate about another axis. This would mean more components, a heavier design, and a more complicated system. The simple act of changing the direction of forward flight eliminated the need for complex frame design.

3.3. Component Selection

3.3.1. Propellers

Based on initial estimates on components and frame design, the total weight of the vehicle was estimated with low fidelity to be three pounds. An intention was to have this project available to future senior design groups for use. This means that there must be more thrust available than just that needed to lift the vehicle. If any controlling instrumentation or any other additions were to be made in the future, the thrust system must have the ability to lift it. This being the case, an original design for six pounds thrust total was a goal. Another goal was for this to be achievable at less than full throttle of the motors. After some rudimentary thrust calculations and some insight from professionals in the field of RC, 14x5.5 inch propellers were chosen.

3.3.2. Motors

With the propellers chosen, a motor had to be chosen that could do two things: the motor had to be able to achieve a high enough RPM to provide the desired thrust, and also had to be able to withstand the torque from the propeller at speed. Some benchmarking with the local hobby store as well as some research into appropriate propeller sizes for different size motors led to the decision to use a 620 kV 1000 W motor. The recommended ESC for pairing with this motor was chosen.

3.3.3. Batteries

With the motor chosen, the battery had to be chosen to produce the desired thrust. The kV rating on a motor represents how many RPMs/Volt introduced to the motor the motor will turn. This was an area that was given a very large safety factor so as to have more power than required, just in case. A 5-cell, 3000 mAh battery was chosen.

3.3.4. Servos

The servos were also chosen with the intent to have more torque than required. Many of these components were chosen with future projects in mind where the weight of the vehicle may very well increase as well as the application of the components. A 8.68 lb·in (10 kg·cm) and 60° rated servo was chosen.

3.4. ESC Configuration

Typically, in any given remote control model, each motor used on the vehicle is connected to its own ESC, which is then attached to its own battery. That is the case for the current prototype vehicle. However, another configuration was studied. This alternative has both motors connected to their respective ESCs, but both ESCs are attached to one battery through the use of a Y-splitter, as seen in Figure 6.

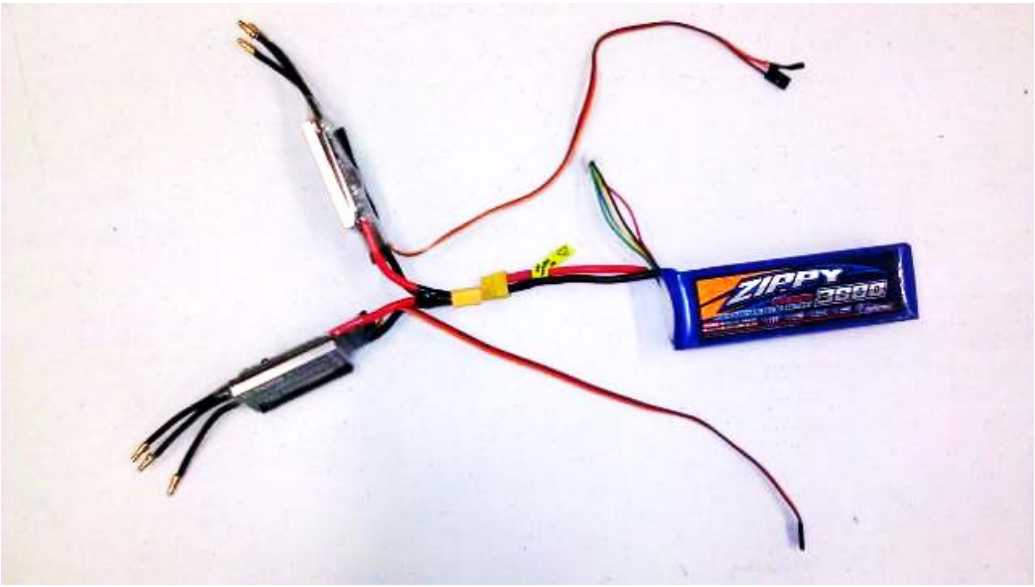

Figure 6: Y-splitter setup

This home-constructed Y-splitter uses one battery and places the ESCs in parallel so that they will, theoretically, always be receiving the same voltage. The RPM of the motors are directly related to the voltage they are receiving, therefore, the Y-splitter allows both motors to constantly be running at the same RPM. Ultimately, this configuration was not used due to the lack of differential thrust control. Ideally, differential thrust control would not be needed if the model was perfectly balanced, manufactured, etc. However, enough error exists in the current prototype that it was determined differential thrust control was necessary, and that cannot be obtained using one power source. Despite not using this configuration, details for the flight tests for the Y-splitter configuration are included in the flight testing section of this report.

Because the Y-splitter theoretically maintains consistent RPM between the two motors, it should maintain equivalent thrust. As such, the Y-splitter represents the ESC configuration for an ideal-case model. As an ideal-case prototype is the eventual goal of this project, this case was simulated in the dynamic model. The results from this simulation are shown in the Modeling and Simulation section of this paper.

3.5 CAD Model

Once the model was designed, the material decided, the orientation established, and the components selected, a Computer Aided Design (CAD) model was created using SolidWorks.

This model, shown in Figure 7 and dimensioned in Figure 8, was used to determine the moments of inertia of the vehicle.

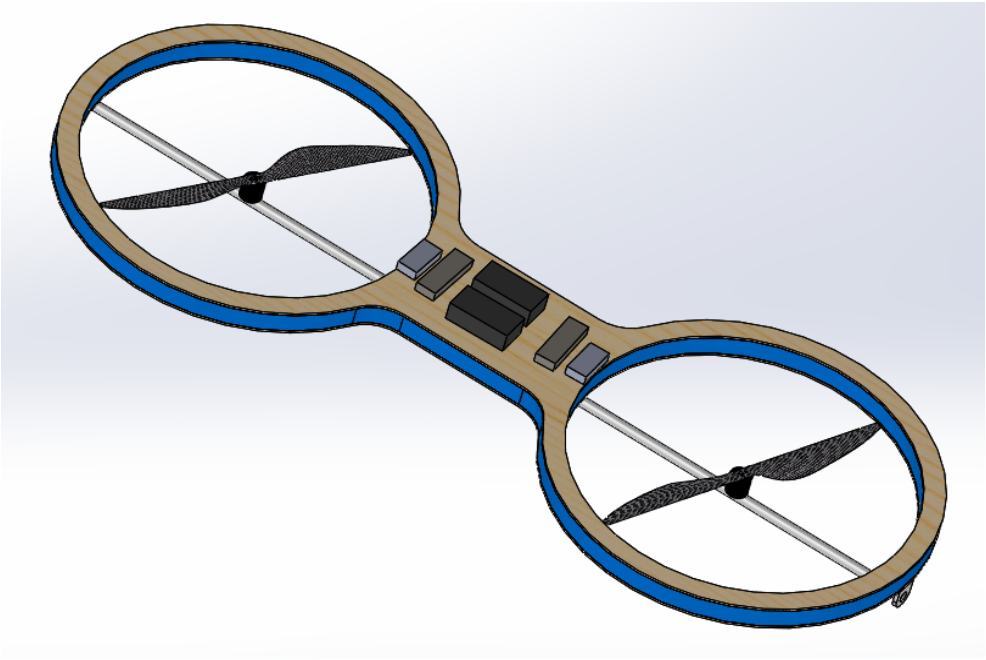

Figure 7: CAD model of vehicle with components

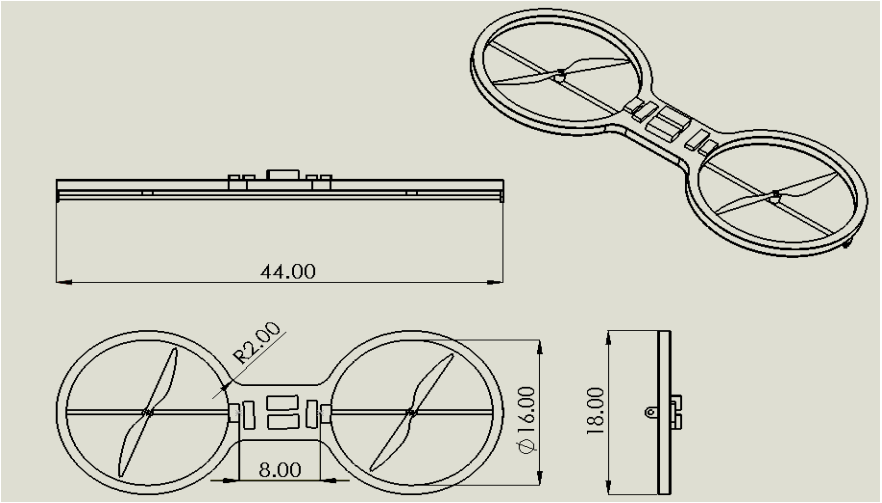

Figure 8: CAD model of vehicle with relevant dimensions

Figure 9 displays the rest of the dimensions and values needed for calculations in the simulation. Moment of inertia is based on mass distribution, therefore, the CAD model did not need to be precise in detail as long as the individual component weights and locations were correct.

Mass properties of Prototype 2
Configuration: Default
Coordinate system: -- default --

Mass = 3.89 pounds

Volume = 212.04 cubic inches

Surface area = 1329.72 square inches

Center of mass: (inches)
X = 12.17
Y = 26.26
Z = 33.97

Principal axes of inertia and principal moments of inertia: (pounds * square
Taken at the center of mass.

Ix = (1.00, 0.00, 0.00)	Px = 39.35
Iy = (0.00, 1.00, 0.00)	Py = 366.08
Iz = (0.00, 0.00, 1.00)	Pz = 399.45

Moments of inertia: (pounds * square inches)
Taken at the center of mass and aligned with the output coordinate system.

Lxx = 39.35	Lxy = 0.25	Lxz = 0.28
Lyx = 0.25	Lyy = 366.08	Lyz = 0.14
Lzx = 0.28	Lzy = 0.14	Lzz = 399.45

Moments of inertia: (pounds * square inches)
Taken at the output coordinate system.

Ixx = 7208.40	Ixy = 1243.37	Ixz = 1608.46
Iyx = 1243.37	Iyy = 5429.99	Iyz = 3469.05
Izx = 1608.46	Izy = 3469.05	Izz = 3657.22

Figure 9: Moments of Inertia of the vehicle

4. Derivation of Equations of Motion

In order to understand the dynamic response of the vehicle, the equations of motion needed to be developed. These equations are based on the degrees of freedom of the vehicle in its environment, and are influenced by the geometry and mass properties of the vehicle. A rigid body that is able to move in three-dimensional space is subject to six degrees of freedom (DOFs). These consist of three translational and three rotational DOFs. The three translational DOFs can be thought of as forward, side to side, and up or down motion. The three rotational DOFs are described by the body's orientation angles. In general aviation, these angles are referred to as roll, pitch, and yaw, so this convention was adopted. From these six DOFs, generalized coordinates were defined, and the system definition was developed. As mentioned above, this design takes advantage of conventional aircraft dynamic terms and nomenclature, so each variable used is common in that way. Listed below is all the nomenclature used in system definition and in all calculations. Accompanying each term is a brief definition.

x_e – *location in X-direction of the inertial frame*

y_e – *location in Y-direction of the inertial frame*

z_e – *location in Z-direction of the inertial frame*

u – *velocity along body frame x-direction*

v – *velocity along body frame y-direction*

z – *velocity along body frame z-direction*

φ – *roll angle*

θ – *pitch angle*

ψ – *yaw angle*

p – *roll rate*

q – *pitch rate*

r – *yaw rate*

Once the DOFs and generalized coordinates were established, it became necessary to define the relative environment around the body. This was done by defining dynamic reference frames. These reference frames were used to relate the motion of the vehicle to the inertial

frame, in all six DOFs. Due to the lack of complexity in the environment of this vehicle, there were only two pertinent frames for this initial analysis. The first frame was the inertial frame, which is defined with unit vectors X, Y, and Z. It is a stationary frame that helps define the three-dimensional space, and it is the frame that all forces are resolved in. The second frame, called the body frame, is the set of unit vectors that define the vehicle. The general convention in aviation is north-east-down (NED), which is to say the body x-direction points in the direction of forward motion, body y-direction points out to the right of the vehicle, and the body z-direction points downward. This set of unit vectors follows the right hand rule. Furthermore, to give an initial reference, the body frame unit vectors are aligned with the inertial frame unit vectors when no rotations have been performed to the body. This concept will be explained in further detail in the following section. A clear representation of each of the orientation angles is given in Figures 10, 11, and 12.

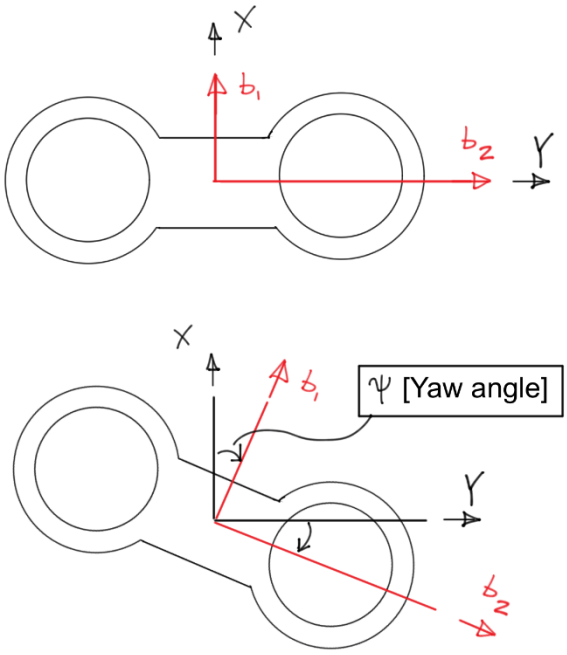

Figure 10: Yaw rotation

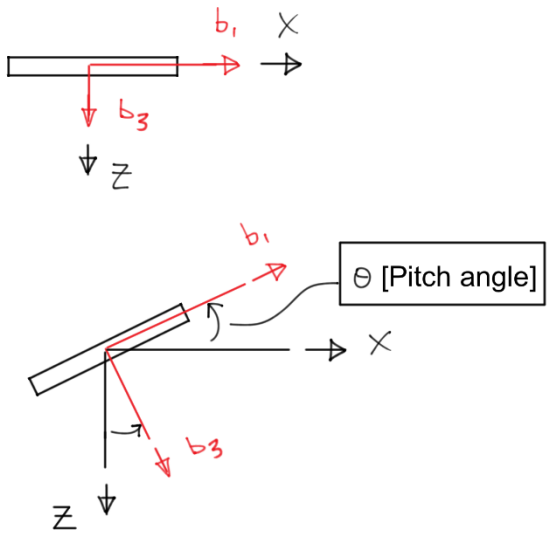

Figure 11: Pitch rotation

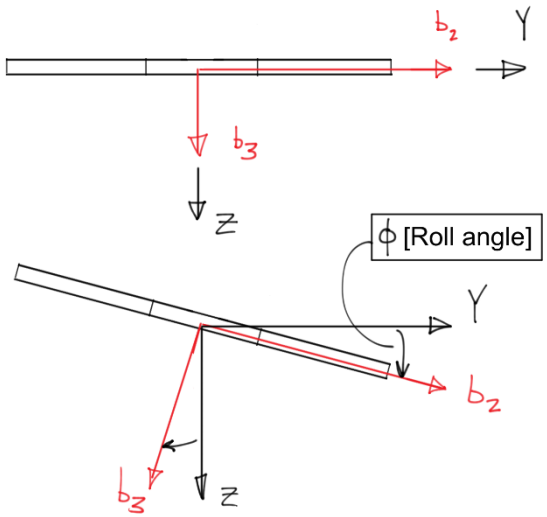

Figure 12: Roll rotation

In order to correlate the body frame with the inertial frame, a 3-2-1 rotation sequence was used. This defines the first rotation as being about the body z-axis, the second about the body y-axis, and the third about the body x-axis. The first rotation, shown in Figure 10, is the rotation that defines the vehicle yaw angle. The second rotation, shown in Figure 11, is the rotation that defines the vehicle pitch angle. The third rotation, shown in Figure 12, is the rotation that defines the vehicle roll angle.

In order to attain a complete unit vector relation from the inertial frame to the body frame, each successive rotation must be described by a transformation matrix. The set of equations below illustrates these three rotations. Since they are sequential, it is necessary to use intermediate frames, described by the *N* and *N'* unit vector sets, to complete the process.

$$R_1: \begin{bmatrix} N_1 \\ N_2 \\ N_3 \end{bmatrix} = \begin{bmatrix} C_\psi & S_\psi & 0 \\ -S_\psi & C_\psi & 0 \\ 0 & 0 & 1 \end{bmatrix} \begin{bmatrix} X \\ Y \\ Z \end{bmatrix} \tag{2}$$

$$R_2: \begin{bmatrix} N_1' \\ N_2' \\ N_3' \end{bmatrix} = \begin{bmatrix} C_\theta & 0 & -S_\theta \\ 0 & 1 & 0 \\ S_\theta & 0 & C_\theta \end{bmatrix} \begin{bmatrix} N_1 \\ N_2 \\ N_3 \end{bmatrix} \tag{3}$$

$$R_3: \begin{bmatrix} b_1 \\ b_2 \\ b_3 \end{bmatrix} = \begin{bmatrix} 1 & 0 & 0 \\ 0 & C_\phi & S_\phi \\ 0 & -S_\phi & C_\phi \end{bmatrix} \begin{bmatrix} N_1' \\ N_2' \\ N_3' \end{bmatrix} \tag{4}$$

Multiplying each of the rotations in order from R_3 to R_1 eliminates the intermediate frames and results with a final transformation matrix that describes the orientation of the body frame with respect to the inertial frame. This matrix is labeled as L_{NB}, because it transforms body frame coordinates into the inertial frame coordinates.

$$L_{NB} = \begin{bmatrix} C_\theta C_\psi & S_\phi S_\theta C_\psi - C_\phi S_\psi & C_\phi S_\theta C_\psi + S_\phi S_\psi \\ C_\theta S_\psi & S_\phi S_\theta S_\psi + C_\phi C_\psi & C_\phi S_\theta S_\psi - S_\phi C_\psi \\ -S_\theta & S_\phi C_\theta & C_\phi C_\theta \end{bmatrix} \tag{5}$$

4.1. Attitude Kinematics

In the interest of building from the ground up, the first two sets of equations are those that describe the kinematics of the vehicle. Each of these two sets contains three equations, one for each of the three dimensions. The kinematics are used to describe the relationship between the vehicle and the inertial frame. Stemming from the previous description of the orientations, it is possible to define the time derivatives of the angles. This is done through the consideration of

simple angular velocities. In three dimensional space, it is convenient to break down complex motion into its individual components. Equation 6 show the basic form of this concept.

$$ {}^{N}\underline{\omega}^{B} = {}^{N}\underline{\omega}^{N'} + {}^{N'}\underline{\omega}^{N''} + {}^{N''}\underline{\omega}^{B} \tag{6} $$

From the 3-2-1 rotation sequence outline above, the angular velocity of the system can be resolved in the same way. The result of the derivation process, expressed in matrix form, is shown in equation 7.

$$ \begin{bmatrix} p \\ q \\ r \end{bmatrix} = \begin{bmatrix} 1 & 0 & -S_{\Phi} \\ 0 & C_{\Phi} & S_{\Phi}C_{\theta} \\ 0 & -S_{\Phi} & C_{\Phi}C_{\theta} \end{bmatrix} \begin{bmatrix} \dot{\Phi} \\ \dot{\theta} \\ \dot{\psi} \end{bmatrix} \tag{7} $$

Recall that the p, q, and r quantities are body frame angular velocities, and the variables that describe the rotations relative to the inertial frame are Φ, θ, and ψ. Thus, rearranging and expanding yields the set of equations that describe the angular kinematics of the body.

$$ \dot{\Phi} = p + (sin\Phi tan\theta)q + (cos\Phi tan\theta)r \tag{8} $$

$$ \dot{\theta} = (cos\Phi)q - (sin\Phi)r \tag{9} $$

$$ \dot{\psi} = (sin\Phi sec\theta)q + (cos\Phi sec\theta)r \tag{10} $$

4.2. Position Kinematics

Since the vehicle is defined as a rigid body, which is essentially a collection of points, one point of interest on the body must be chosen to resolve the translational kinematics. The point selected on this vehicle corresponded with the center of gravity (CG). This is convenient in a number of ways, but the most general reason is that the location of the CG is also where the body accelerations are later resolved for the dynamic calculations. Much like the attitude kinematics, the second set of kinematic equations relates the position of the CG, and are derived from velocity of the CG with respect to the inertial frame. Again using the transformation matrix from above, the set of equations is expressed as,

$$ {}^{N}v_{N}^{B^*} = L_{NB} \cdot {}^{N}v_{B}^{B^*} \tag{11} $$

$$ \begin{bmatrix} \dot{x}_e \\ \dot{y}_e \\ \dot{z}_e \end{bmatrix} = \begin{bmatrix} C_\theta C_\psi & S_\Phi S_\theta C_\psi - C_\Phi S_\psi & C_\Phi S_\theta C_\psi + S_\Phi S_\psi \\ C_\theta S_\psi & S_\Phi S_\theta S_\psi + C_\Phi C_\psi & C_\Phi S_\theta S_\psi - S_\Phi C_\psi \\ -S_\theta & S_\Phi C_\theta & C_\Phi C_\theta \end{bmatrix} \begin{bmatrix} u \\ v \\ w \end{bmatrix} \tag{12} $$

The important point to note is that the velocity term is in fact the same quantity expressed in two separate frames. The transformation comes when choosing the frame of interest. Since the goal is to track the motion of the vehicle from an inertial standpoint, the equations need to be expressed in the inertial frame. Expanding the above equation set reveals three distinct position kinematic equations.

$$ \dot{x}_e = (C_\theta C_\psi)u + (S_\Phi S_\theta C_\psi - C_\Phi S_\psi)v + (C_\Phi S_\theta C_\psi + S_\Phi S_\psi)w \tag{13} $$

$$ \dot{y}_e = (C_\theta S_\psi)u + (S_\Phi S_\theta S_\psi + C_\Phi C_\psi)v + (C_\Phi S_\theta S_\psi - S_\Phi C_\psi)w \tag{14} $$

$$ \dot{z}_e = (-S_\theta)u + (S_\Phi C_\theta)v + (C_\Phi C_\theta)w \tag{15} $$

4.3. Translational Dynamics

Once the two sets of kinematic equations were derived, the next steps were to formulate the two set of equations that correspond with the dynamics of the vehicle. To begin, the translational dynamics were produced using the first principles of Newton's laws. The CG was chosen as the point about which to derive the acceleration, as it is assumed that all forces can be summed at that point. Equation 16 gives the basic form of Newton's second law, while equation 17 exhibits an expanded form of the acceleration term that specifically relates to this vehicle.

$$ \sum \underline{F} = m\,{}^{N}\vec{\underline{a}}^{B^*} \tag{16} $$

$$ {}^{N}\underline{a}^{B^*} = {}^{N}\frac{d}{dt}\left({}^{N}\underline{V}_{B}^{B^*}\right) = {}^{B}\frac{d}{dt}\left({}^{N}\underline{V}_{B}^{B^*}\right) + \left({}^{N}\underline{\omega}^{B} \times {}^{N}\underline{V}_{B}^{B^*}\right) \tag{17} $$

When differentiating to get the acceleration term, it is crucial to define the frame with respect to which it is being derived. It is desirable to solve for inertial forces, therefore the terms were differentiated with respect to the inertial frame. However, the velocity terms are expressed in body frame components, and in order to do this the method often called "The Derivative Rule" was applied. This method defines the differentiation of a vector in two different frames, and is shown in equation 17. The expanded matrix form of this equation is shown below.

$$ {}^{N}\underline{a}^{B^*} = \begin{bmatrix} \dot{u} \\ \dot{v} \\ \dot{w} \end{bmatrix} + \begin{bmatrix} 0 & -r & q \\ r & 0 & -p \\ -q & p & 0 \end{bmatrix} \begin{bmatrix} u \\ v \\ w \end{bmatrix} \tag{18} $$

Next, the forces that act on the vehicle were defined and included in the overall set of equations. Because this vehicle was assumed to be moderately unstable, it was expected to operate at slow speeds, and thus aerodynamics forces were assumed to be negligible. Other forces acting on the body include the weight, thrust force produced by the spinning propellers, and the force of the landing gear, which disappear once the craft is airborne, so those too were neglected. A summary of these forces is shown below in equations 19 and 20.

$$ \sum \underline{F} = \underline{T} + m\underline{g} + \underline{F}_{L/G} \tag{19} $$

$$ \sum \underline{F} = \begin{bmatrix} T_x \\ T_y \\ T_z \end{bmatrix} + L_{BN} \begin{bmatrix} 0 \\ 0 \\ mg \end{bmatrix} + 0 \tag{20} $$

The final consideration of external forces on the vehicle were those from close interaction with ground, commonly referred to as "ground effect". This is an aerodynamic phenomena that plays into the operation of flight vehicles that are within a certain proximity to the ground during operation. While it is a major contributing factor in the project prototype, it is also very complex and difficult to describe. After a good deal of research, it was determined that an accurate mathematical representation of ground effect was outside the scope of this report, and therefore it was not added to the equations. [6] This is noted as being a large source of error in the simulation procedure and certainly one of the main topics for increasing the accuracy of the model.

Lastly, equations 18 and 20 were combined and rearranged to solve for the three acceleration components of the center of gravity. This resulting set of equations makes up the governing principles of the translational dynamic motion. Equation 21 shows the final matrix form, while with equations 22, 23, and 24 are the expanded form for each component.

$$\begin{bmatrix} \dot{u} \\ \dot{v} \\ \dot{w} \end{bmatrix} = -\begin{bmatrix} 0 & -r & q \\ r & 0 & -p \\ -q & p & 0 \end{bmatrix} \begin{bmatrix} u \\ v \\ w \end{bmatrix} + \begin{bmatrix} T_x/m \\ T_y/m \\ T_z/m \end{bmatrix} + g \begin{bmatrix} -S_\theta \\ S_\phi C_\theta \\ C_\phi C_\theta \end{bmatrix} \tag{21}$$

$$\dot{u} = rv - qw - g(sin\theta) + \frac{T_x}{m} \tag{22}$$

$$\dot{v} = pw - ru + g(sin\phi\ cos\theta) + \frac{T_y}{m} \tag{23}$$

$$\dot{w} = qu - rv + g(cos\phi\ cos\theta) + \frac{T_z}{m} \tag{24}$$

4.4. Rotational Dynamics

The final set of equations are those corresponding with the rotational dynamics of the vehicle. These are derived from Euler's equation, which states the sum of the moments about a certain point is equal to the time rate change of the angular momentums. This can be summarized in its most general form as,

$$\underline{M}^{B^*} = {}^{N}\frac{d}{dt}\left({}^{N}\underline{H}^{B^*}\right) = {}^{B}\frac{d}{dt}\left({}^{N}\underline{H}^{B^*}\right) + \left({}^{N}\underline{\omega}^{B} \times {}^{N}\underline{H}^{B^*}\right) \tag{25}$$

Due to the relationship between the two frames, it is necessary to resolve all terms in the body frame. In this way all inertia components can be evaluated as constant because the body is considered rigid and fixed in its respective frame. By expanding and rearranging the terms to solve for the angular accelerations, the following equation is formed.

$$\begin{bmatrix} \dot{p} \\ \dot{q} \\ \dot{r} \end{bmatrix} = -\begin{bmatrix} {}^{1}/_{I_{xx}} & 0 & 0 \\ 0 & {}^{1}/_{I_{yy}} & 0 \\ 0 & 0 & {}^{1}/_{I_{zz}} \end{bmatrix} \begin{bmatrix} -rqI_{yy} + qrI_{zz} \\ rpI_{xx} - prI_{zz} \\ -qpI_{xx} + pqI_{yy} \end{bmatrix} + \begin{bmatrix} {}^{L}/_{I_{xx}} \\ {}^{M}/_{I_{yy}} \\ {}^{N}/_{I_{zz}} \end{bmatrix} \tag{26}$$

In this equation, one can notice the diagonal nature of the inertia matrix. This is based on the assumption of having a vehicle with multiple planes of symmetry, which indicates that all products of inertia are zero, leaving only the principal moments of inertia. Also, the *L*, *M*, and *N* terms represent the external moments about the CG. These moments come from the thrust forces and the torques output by the motors. For this vehicle, there are only external moments in the roll and yaw directions. The two propellers are aligned in the body y-axis, so the thrust only has a moment arm that contributes to roll. Likewise, the propellers rotate mostly in the body z-direction, therefore the reaction torque is also about this direction. This is an important point because it indicated that the thrusts and angular velocity of the propellers need to be equal in order to maintain angular stability. The expanded form of the rotational dynamic equation set is,

$$\dot{p} = qr\frac{I_{yy} - I_{zz}}{I_{xx}} + \frac{L}{I_{xx}} \tag{27}$$

$$\dot{q} = pr\frac{I_{zz} - I_{xx}}{I_{yy}} + \frac{M}{I_{yy}} \tag{28}$$

$$\dot{r} = pq\frac{I_{xx} - I_{yy}}{I_{zz}} + \frac{N}{I_{zz}} \tag{29}$$

The entire set of governing equations for the motion of this vehicle are twelve nonlinear, first-order differential equations. These equations are the building blocks for computationally simulating the system. However, one of the future aims of this project is to incorporate a control system to compensate for the inherent instability and allow the vehicle to be piloted effectively. The conventional way to approach such an issue is with a linear controller. Therefore, the twelve equations were linearized about two primary equilibrium states and evaluated using linear simulation techniques.

5. Equation Linearization

In order to begin linearizing the equations of motion, specific equilibrium states must be defined. For simplicity, two cases were chosen for this model. The first was that of simple hovering flight and the second considers a constant forward flight. The respective variables that define these cases are,

Hovering:

$$\begin{array}{lllll} \dot{u}=0 & \dot{p}=0 & u=0 & p=0 & \Phi=0 \\ \dot{v}=0 & \dot{q}=0 & v=0 & q=0 & \theta=0 \\ \dot{w}=0 & \dot{r}=0 & w=0 & r=0 & \psi\neq 0 \end{array}$$

Forward Flight:

$$\begin{array}{lllll} \dot{u}=0 & \dot{p}=0 & u\neq 0 & p=0 & \Phi=0 \\ \dot{v}=0 & \dot{q}=0 & v=0 & q=0 & \theta=0 \\ \dot{w}=0 & \dot{r}=0 & w=0 & r=0 & \psi\neq 0 \end{array}$$

Linearization was conducted by using small perturbation theory, which applies a Taylor series expansion around the equilibrium. Therefore, all responses from the simulations will be with respect to the perturbed state variables. Each of the twelve equations were linearized for each case, and the derivations of which can be found in Appendix A. Results for the hovering case include:

$$\Delta\dot{u} = -g\Delta\theta + \frac{1}{m}\Delta T_x \tag{30}$$

$$\Delta\dot{v} = \frac{1}{m}\Delta T_y + g\Delta\Phi \tag{31}$$

$$\Delta\dot{w} = \frac{1}{m}\Delta T_z + g \tag{32}$$

$$\Delta\dot{p} = \frac{\Delta L}{I_{xx}} \tag{33}$$

$$\Delta\dot{q} = \frac{\Delta M}{I_{yy}} \tag{34}$$

$$\Delta\dot{r} = \frac{\Delta N}{I_{zz}} \tag{35}$$

$$\Delta\dot{x}_e = (cos\psi_0)\Delta u + (sin\psi_0)\Delta v \tag{36}$$

$$\Delta\dot{y}_e = (sin\psi_0)\Delta u + (cos\psi_0)\Delta v \tag{37}$$

$$\Delta\dot{z}_e = \Delta w \tag{38}$$

$$\Delta\dot{\Phi} = \Delta p \tag{39}$$

$$\Delta\dot{\theta} = \Delta q \tag{40}$$

$$\Delta\dot{\psi} = \Delta r \tag{41}$$

Similar procedures were conducted for the second case to obtain a new set of equation for that equilibrium position. Because the motion is quite simple, the results are the same for a number of the variables. The forward flight case equations are summarized as:

$$\Delta\dot{u} = -g\Delta\theta + \frac{1}{m}\Delta T_x \tag{42}$$

$$\Delta\dot{v} = -\Delta r u_0 + \frac{1}{m}\Delta T_y + g\Delta\Phi \tag{43}$$

$$\Delta\dot{w} = \Delta q u_0 + \frac{1}{m}\Delta T_z + g \tag{44}$$

$$\Delta\dot{p} = \frac{\Delta L}{I_{xx}} \tag{45}$$

$$\Delta\dot{q} = \frac{\Delta M}{I_{yy}} \tag{46}$$

$$\Delta\dot{r} = \frac{\Delta N}{I_{zz}} \tag{47}$$

$$\Delta\dot{x}_e = (cos\psi_0)u_0 - (sin\psi_0 u_0)\Delta\psi + (cos\psi_0)\Delta u - (sin\psi_0)\Delta v \tag{48}$$

$$\Delta\dot{y}_e = (sin\psi_0)u_0 + (sin\psi_0)\Delta u + (cos\psi_0 u_0)\Delta\psi + (cos\psi_0)\Delta v \tag{49}$$

$$\Delta\dot{z}_e = -\Delta\theta u_0 + \Delta w \tag{50}$$

$$\Delta\dot{\Phi} = \Delta p \tag{51}$$

$$\Delta\dot{\theta} = \Delta q \tag{52}$$

$$\Delta\dot{\psi} = \Delta r \tag{53}$$

With these two complete sets of equations, the system can be analyzed to determine how it will dynamically respond to given inputs or disturbances. These simulations, which are described in the following section, provide a basis by which a physical prototype may be compared.

6. Modeling and Simulation

6.1. Building the Model

The system was modeled using the engineering software, MATLAB. Since the equations of motion were linearized about various equilibrium positions, a linear simulation operator was used to show the response of the system with many different inputs. These inputs included step, doublet, and impulse inputs. Analysis of the response with each input yields a prediction of the expected motion of the vehicle. This is extremely helpful when something needs to be fixed, changed, or possibly added to alter the motion seen during flight testing, because time and money do not need to be spent working on the prototype.

Three separate models were built to simulate the motion of the vehicle. The first model represents the ideal situation. This model assumes equal thrust from each rotor, and the equations were linearized about hovering flight. The second model, also linearized about hovering flight, considers asymmetric servo deflection and thrust between the rotors. The third model also considers asymmetry, but was linearized about a forward flight condition where there is an initial velocity in the body-x direction. Using these three models, a comprehensive analysis was made about the motion of the system, and conclusions and recommendations were drawn about the model.

6.2. Simulation Results Discussion

6.2.1. Thrust vs. RPM Curve

The thrust curve shown in Figure 13 was used to preliminarily choose propellers and motors based on the desired lift for the prototype. [7] This curve was also used in the simulation for determining the thrust from each propeller along with its associated torque.

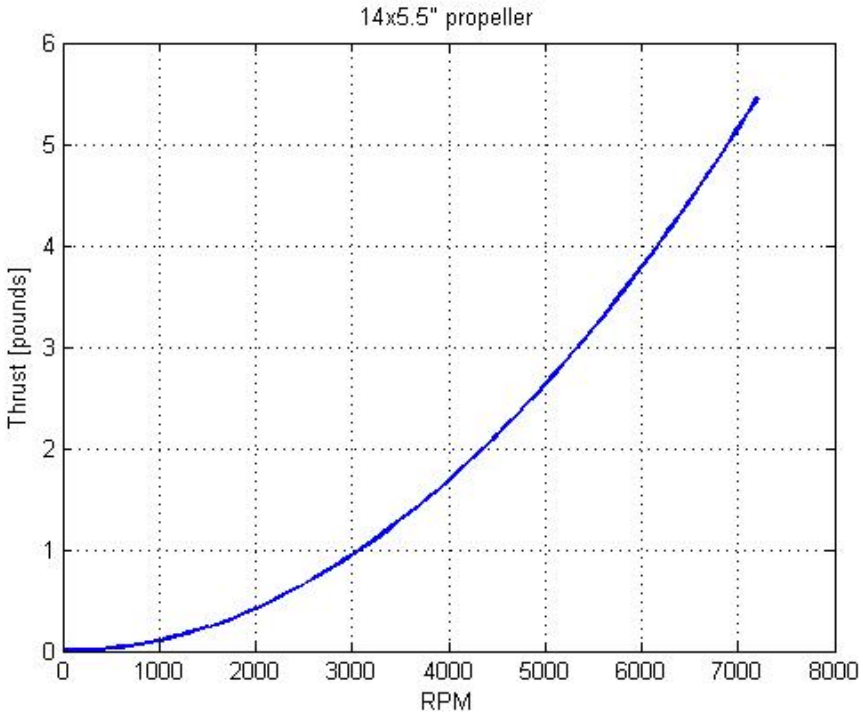

Figure 13: Thrust curve

6.2.2. Ideal Flight Scenario

The ideal flight scenario utilized the Y-split ESC configuration. In the model, this translates to equal thrust from both propellers. This is a very strong assumption. In reality, the thrust from each propeller is not exactly identical due to irregularities between the two ESCs and the two motors. These irregularities include differences in wiring within the motors, differences in internal resistance in each component of the ESC, etc. The ideal condition disregards these aspects, and assumes that each motor sees the exact same voltage, and produces the exact same thrust. The inputs investigated for this scenario included step and doublet inputs for two flight cases: forward motion, and turning motion. Both flight cases started in hovering motion, and the inputs were introduced at the 1 second time interval.

Ideal flight scenario – forward motion step input

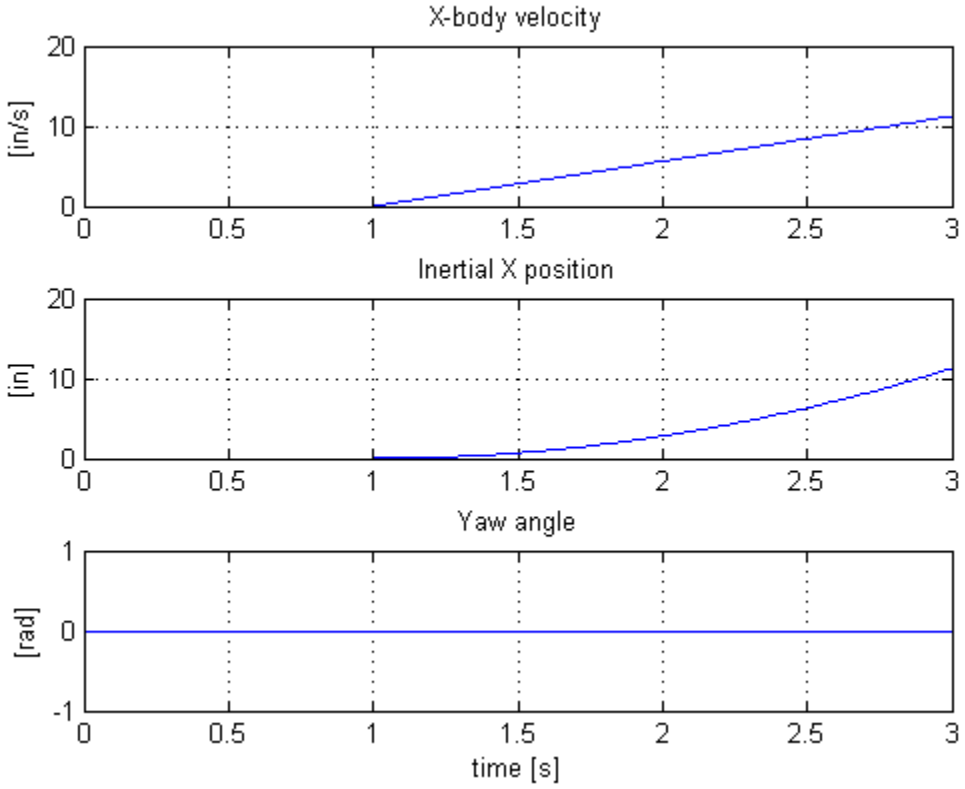

Figure 14: Ideal flight scenario with a forward motion step input

For a forward flight step input, the servos were deflected 5° in the same direction. The first subplot in Figure 14 shows the linear motion in the body x-direction created by this input while the second and third subplots show the inertial X-position and the yaw angle, respectively. The inertial X-position is not linear because the vehicle is accelerating. The yaw angle remains constant at 0° because of the ideal nature of this scenario. Equal thrust from counter-rotating propellers yields no rotational moment acting upon the vehicle, resulting in forward motion only.

Ideal flight scenario – forward motion doublet input

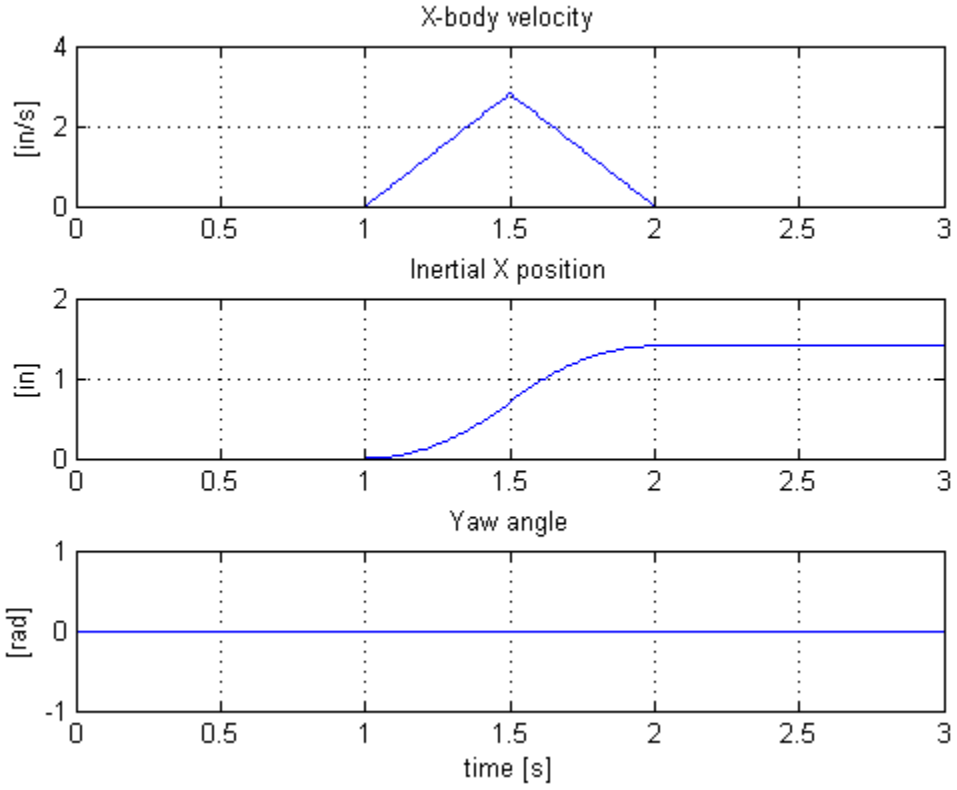

Figure 15: Ideal flight scenario with a forward motion doublet input

For the forward flight with a doublet input, the servos were deflected 5° in the same direction, and half of a second later, they were deflected 5° in the opposite direction. The first subplot in Figure 15 shows the vehicle velocity increasing and then decreasing in the body x-direction, while the second and third subplots again show the inertial X-position and the yaw angle, respectively. The inertial X-position shows the vehicle accelerating and moving forward, then, at one and a half seconds, decelerating while still moving forward until the vehicle comes to a stop. Again, the yaw angle is 0° because this is an ideal scenario, resulting in only forward motion.

Ideal flight scenario – turning motion step input

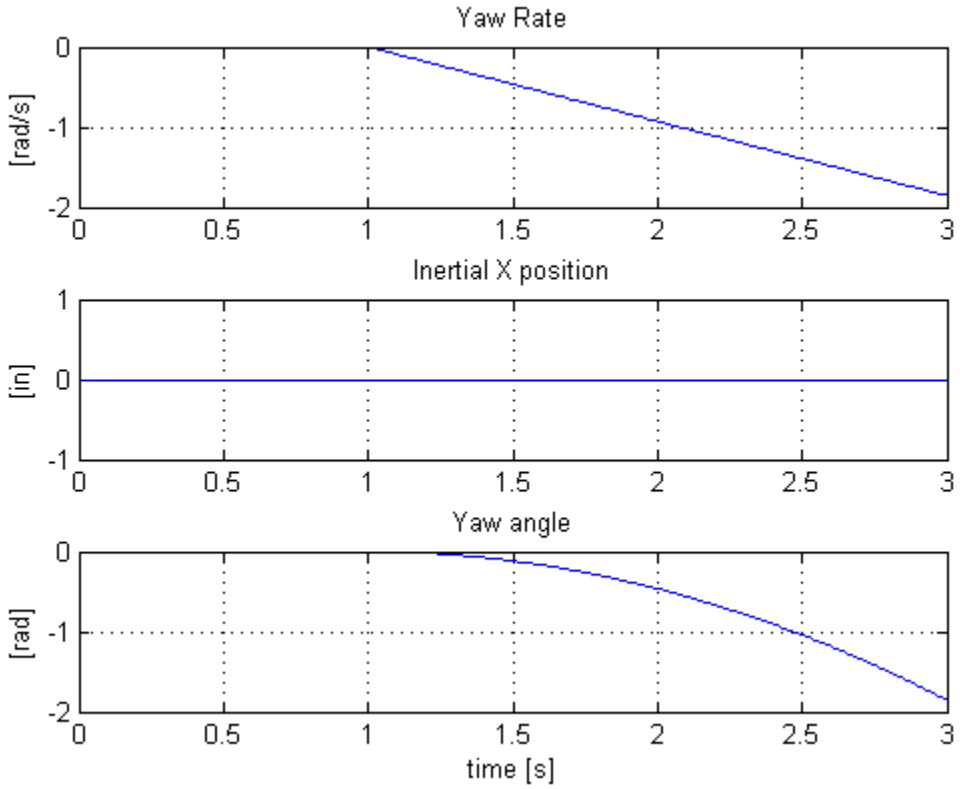

Figure 16: Ideal flight scenario with a forward motion doublet input

In the ideal turning flight case, the servos were again deflected 5°, only now they are being deflected in opposite directions to induce a yawing moment about the CG of the vehicle. Ideally, there is no translational motion, as seen in the second subplot in Figure 16. The first subplot shows the yaw rate, and the third subplot shows the yaw angle. Since this is a step input, yaw rate and yaw angle are expected to change over time, meaning there is a constant angular acceleration about the body z-direction, through the CG of the vehicle.

Ideal flight scenario – turning motion doublet input

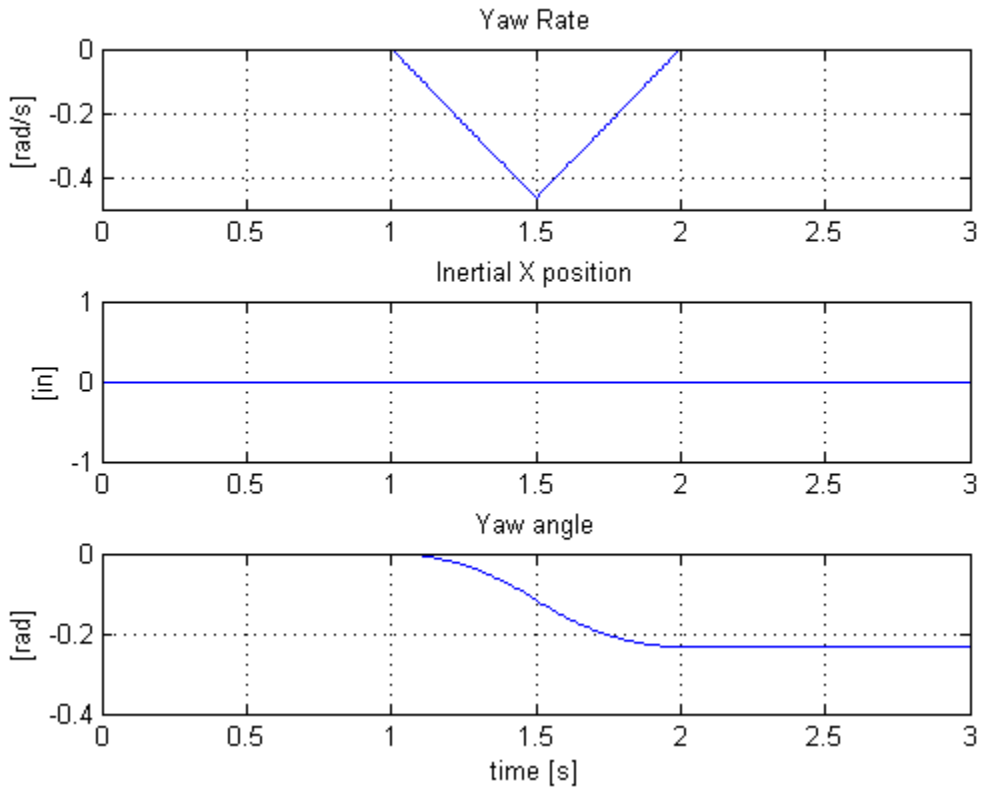

Figure 17: Ideal flight scenario with a turning motion doublet input

For the ideal turning case with a doublet input, the servos were deflected 5° in opposing directions, and then these directions were switched. This induces a yawing moment about the CG of the vehicle in one direction, and then when the servo deflections are switched, the direction of this yawing moment changes to oppose the motion created by the first portion of the doublet input. Since these moments are of equal magnitude and for equal periods of time, the vehicle begins to angularly accelerate and then angularly decelerate, bringing it to a stop at a different yaw angle, as seen in the third subplot of Figure 17. The first and second subplots show the yaw rate and inertial X-position, respectively. As this is an ideal scenario, no translational motion is expected, which is why inertial X-position remains constant.

6.2.3. Non-Ideal Flight Scenario: Differential Thrust and Servo Perturbation

While all the plots above were for an ideal scenario where thrust generated from each propeller was identical, and the servos deflected equally, all of the following plots are for non-ideal scenarios and are more representative of the prototype vehicle. These plots all include a perturbation that may occur during flight testing. One of these perturbations is a thrust perturbation on one of the rotors. This is simulated because testing showed that the RPMs of the motors were never perfectly matched, resulting in unequal thrusts. Servo perturbations were also simulated with unequal thrusts to demonstrate what would happen if the vehicle attempted to move forward or turn in the real model. Each of these perturbations occur at one second and are impulse perturbations, lasting for only one tenth of a second.

Something else to note about the following plots is that these are the results of a linear simulation trying to simulate a nonlinear system. As such, the results closely resemble the actual response of the system only for a short period of time. As time increases, the linear results will become more and more erroneous compared to the actual response of the system. The non-linearity of the system is due to factors such as gravity, ground effect, and low fidelity manufacturing. The reason a linear simulation was used was for future application of a linear controller. This controller would be based on the linear simulation results and respond very close to the time of perturbation where the linear result is still close to the actual response of the system.

Non-ideal flight scenario – hovering flight with an impulse thrust perturbation on one propeller

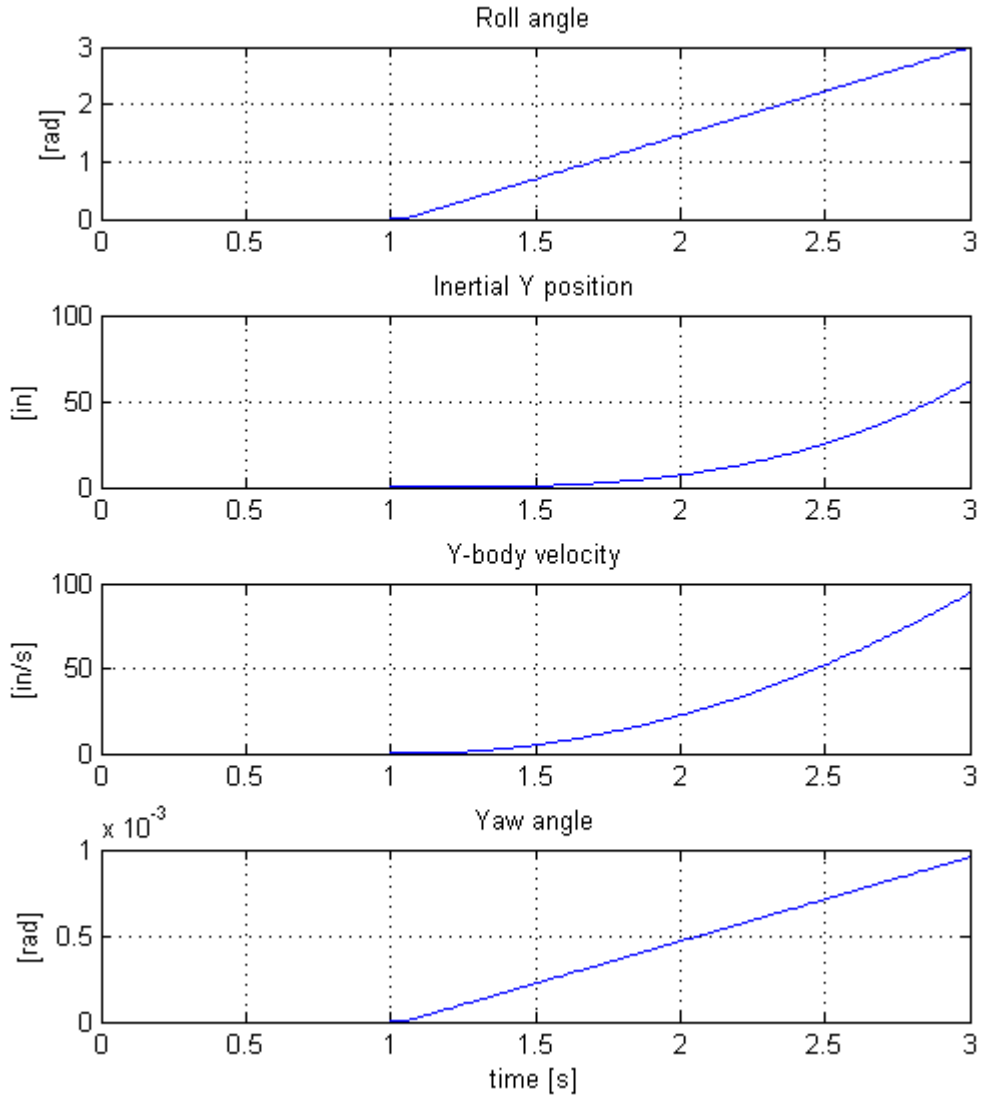

Figure 18: Non-ideal flight scenario with an impulse thrust perturbation during hovering flight

Figure 18 illustrates the motion of a thrust perturbation while the vehicle is simply hovering. A small increase in the thrust in one of the rotors leads to instabilities in both rolling motion and yawing motion. The increased rolling moment about the body x-axis is due to the differential thrust. The magnitude of this rolling moment is rather large and results in a large roll angle. The induced yawing moment is a result of increased angular momentum from the propeller rotating at a higher RPM. The magnitude of this yawing moment is very small, since

the increase in angular momentum is very small. This is seen in the fourth subplot of Figure 18. The first, second, and third subplots show the roll angle, inertial Y-position, and inertial X-position, respectively.

Non-ideal flight scenario – hovering flight with an impulse servo angle perturbation

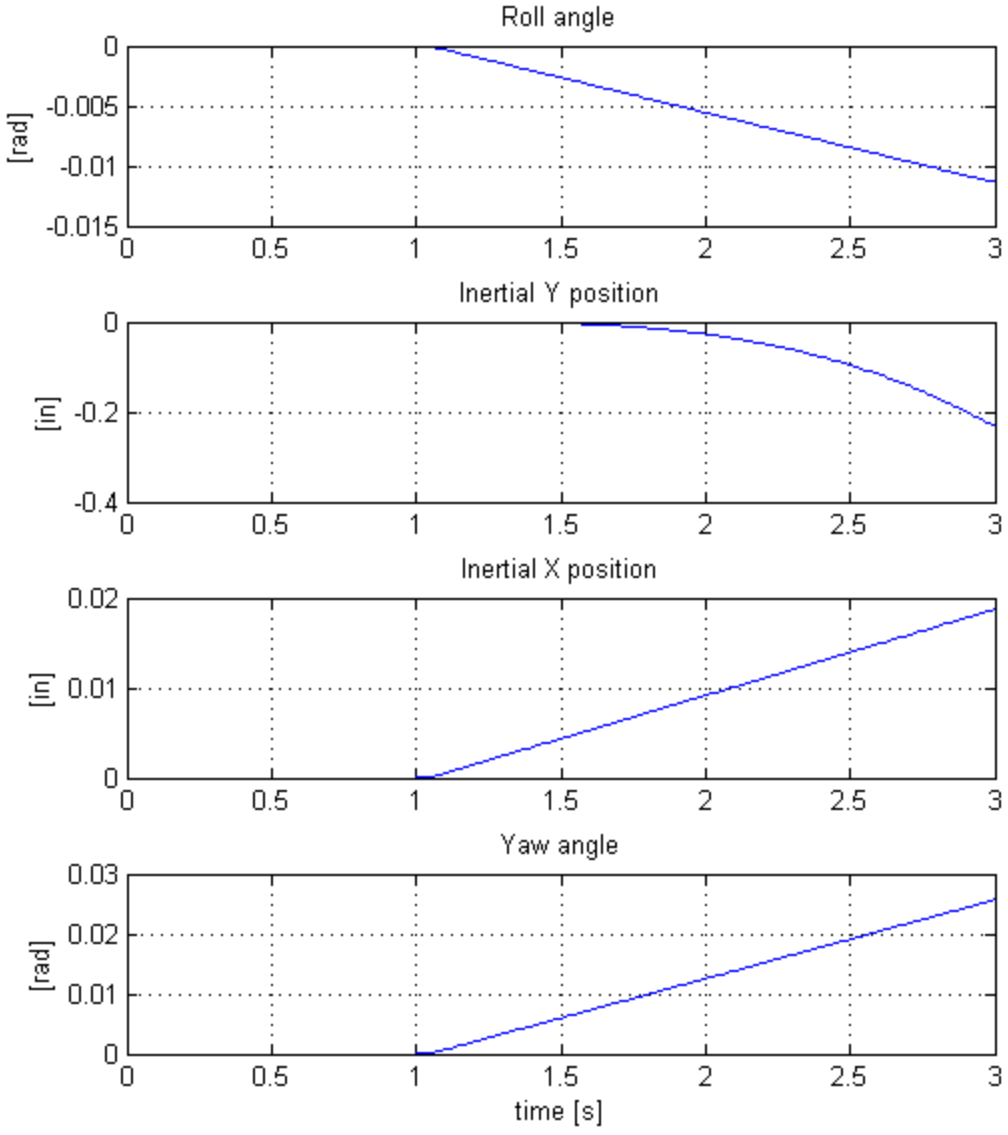

Figure 19: Non-ideal flight scenario with an impulse servo perturbation during hovering flight

Figure 19 shows the vehicle starting from a hover with one servo deflecting 5°. This represents the error in servo deflection in general when the servos deflect at slightly different angles, whether that be in forward or turning motion. As seen in the first subplot, this results in a small rolling motion. The deflected rotor will produce less downward thrust than the other now that its thrust has been vectored and has components in both the body x-direction and the negative body z-direction. This vectoring of thrust also results in yawing, which can be visualized in the fourth subplot. These rolling and yawing motions will result in motion in the inertial-Y and inertial-X directions as seen in the second and third subplots.

Non-ideal flight scenario – forward flight with an impulse thrust perturbation on one propeller

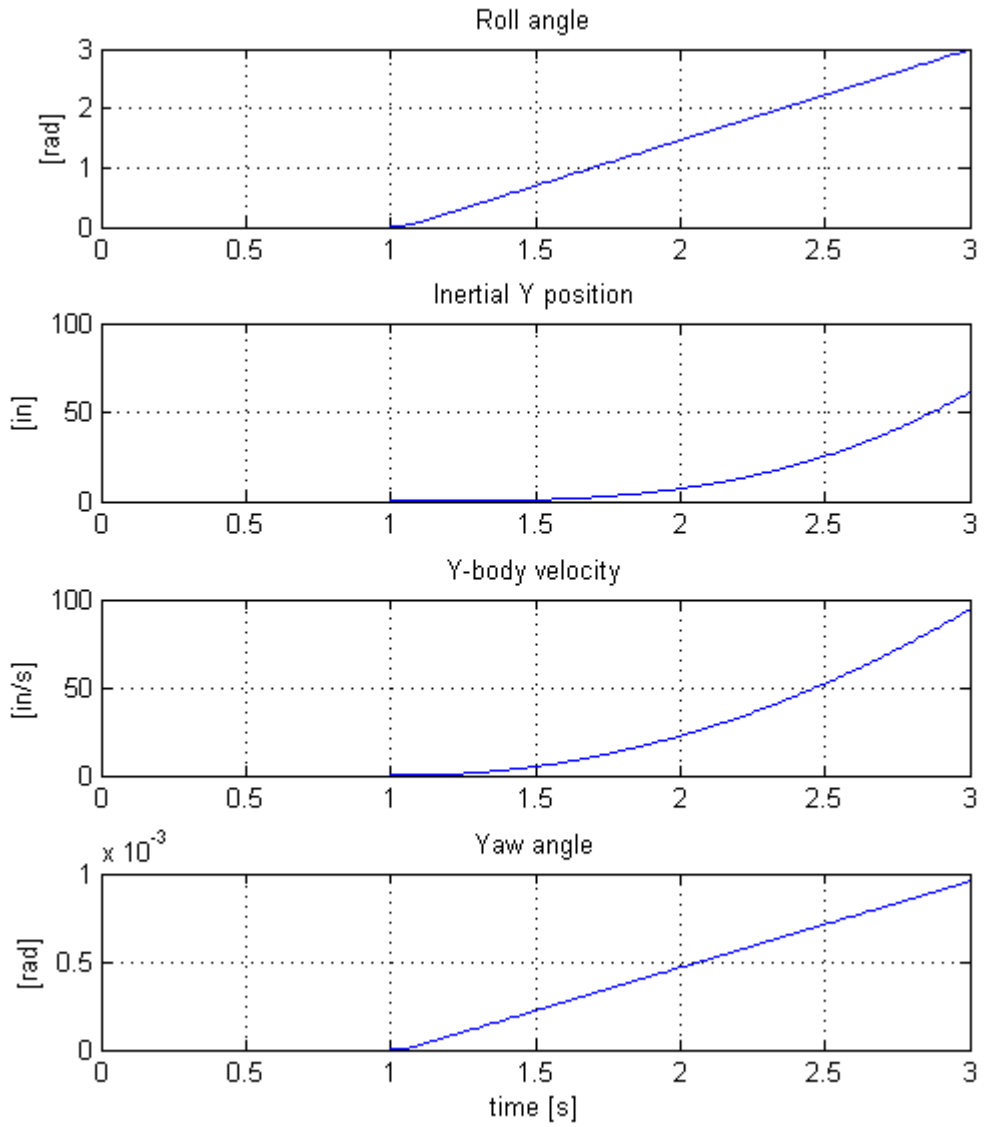

Figure 20: Non-ideal flight scenario with an impulse thrust perturbation during forward flight

In Figure 20, the vehicle is initially moving forward at one inch per second when a thrust perturbation occurs, creating differential thrust. This again results in rolling and yawing motion accompanied by a change in inertial Y-position and body y-velocity due to the different thrusts whilst moving forward. These are seen in the second and third subplots in Figure 20. Similar to the hovering case for the same input, the magnitude of yaw moment created is not very high,

resulting in a slight but constant yaw angle increase. The magnitude of increase in the roll angle is much larger however. This shows just how much the differential thrust can alter the motion of the vehicle. These are seen in the first and fourth subplots in Figure 20.

Non-ideal flight scenario – forward flight with an impulse servo angle perturbation

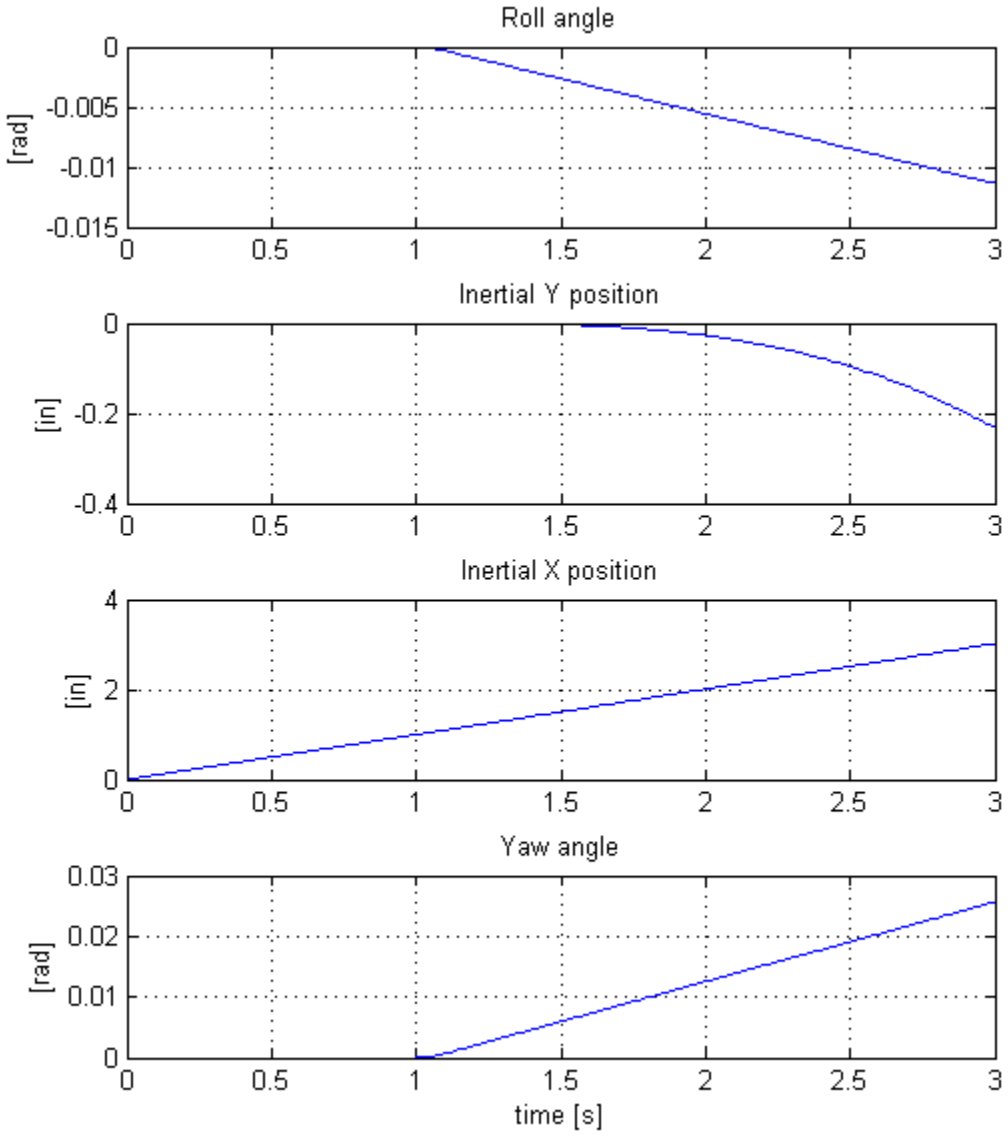

Figure 21: Non-ideal flight scenario with an impulse servo perturbation during forward flight

The plots in Figure 21 simulate one servo deflecting 5° while the vehicle is moving forward at a rate of one inch per second. The results are very similar to Figure 19 where the same input is being used but at the hovering state. As seen in the first and fourth subplots in Figure 21, the vehicle begins to roll and yaw slightly. Once the servo deflects, the component of thrust in the body x-direction increases and the component in the body z-direction decreases, causing the yawing motion and rolling motion, respectively. The inertial Y-position and inertial X-position can be seen in the second and third subplots, respectively.

7. Testing

7.1. Structural Testing

A test was developed, with the setup shown in Figure 22, to test the strength of the current plywood frame in comparison to the old hardboard frame. This test involved placing the ends of each frame on blocks above the ground, measuring the distance the frame lies from the ground, adding a five pound weight to the middle of the frame, and measuring the new distance the frame lies from the ground. By doing this, the deflection of each frame from a five pound weight could be observed to develop a general understanding of the differences in strength between the two frames.

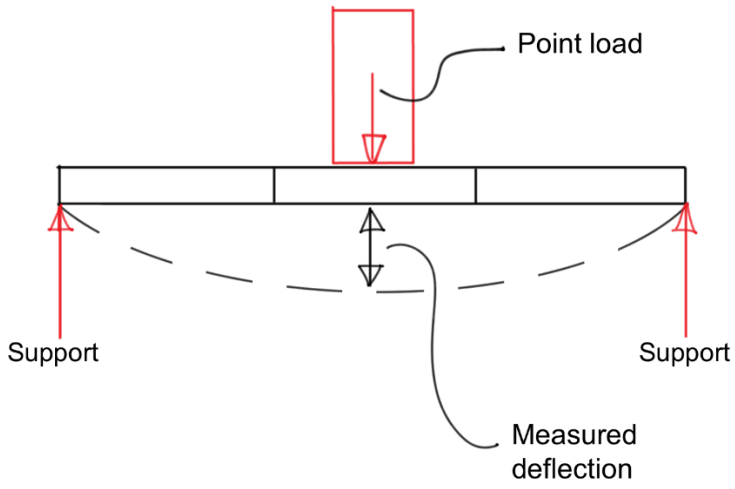

Figure 22: Deflection test setup

Figure 23: Initial (left) and final (right) deflection of frame 1

From Figure 23, it can be seen that the bottom of frame 1 initially sat 7 inches from the ground. After a five pound weight was added the bottom of the frame was 5.75 inches above the ground. This means a 1.25 inch deflection was observed.

Figure 24: Initial (left) and final (right) deflection of frame 2

From Figure 24, it can be seen that the bottom of frame 2 initially sat 7.25 inches from the ground. After a five pound weight was added the bottom of the frame was 6.75 inches above the ground. Therefore, a 0.5 inch deflection was observed.

By changing the material and geometry used in the construction of the frame, strength was increased by 60%. Also, the initial frame weighed 1.43 lbs while the final frame weighed 1.29 lbs. This results in a 10% decrease in weight. This test proves that the second frame, designed with more optimal materials, was both stronger and lighter than the initial design. These improvements were in part due to a purely material increase in strength from hardwood to plywood because plywood has a higher modulus of elasticity. The other large contribution to the decreased deflection under bending was the added distance between the plywood sheets compared to the hardboard sheets. As mentioned earlier, this added distance increased the moment of inertia and brought the bending stiffness of the plywood frame to nearly five times that of the hardboard.

7.2. Flight Testing

Once the frame was constructed, all the components were assembled and the model was flight tested. A number of flight tests were conducted and these tests brought to light a few issues with the design.

Low precision manufacturing yielded a need to trim the base angle of deflection for the servos so as to prevent the model from moving translationally or rotationally when it is meant to be in hovering condition. The battery also had to be moved around the center plate of the frame in order to change the moment of the system and balance it out. The batteries essentially acted as means of changing the center of mass of the system in order to more closely emulate the model that was developed in SolidWorks. There were also a number of things that could not be changed by such easy means. Despite the Y-splitter doing its job and sending a similar signal to each of the motors, there seemed to be a lag in one of the motors. In flight, this translated to one of the rotors spinning faster than the other. This differential RPM lead to more thrust coming up from one rotor as well as a higher angular momentum. This made the model roll about its x-body-axis as well as yaw about its z-body-axis, as shown in Figure 25.

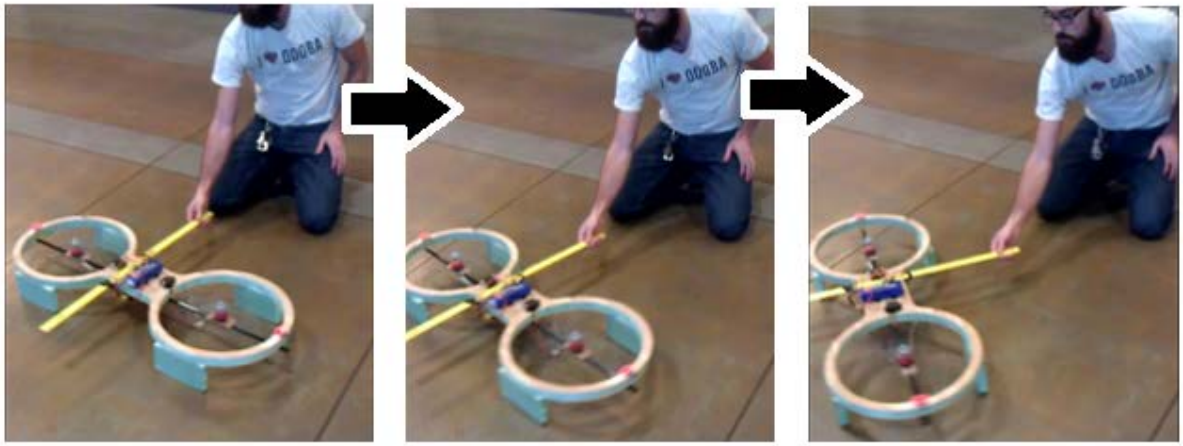

Figure 25: Example of translational and rotational movement in testing

By moving the batteries and controlling the deflection of the servos, both of these problems were temporarily fixed in order to get thrust verification, i.e. confirmation that the rotor/motor/battery setup used could indeed lift the vehicle. This involved a five pound weight being placed on the frame and subsequently lifted off the ground by the vehicle. For a more permanent fix, the controller was programmed to offset the lag in the one motor.

A more hazardous problem encountered during initial flight testing was vibrational issues. Two times, while getting up to speed, a resonant frequency was reached with the servo/spar setup. The initial idea, shown in Figure 26, was to have the mounting spar rotate about the center of the propeller. This left the mounting spar unfixed due to its need to translate in order to lend rotation. The vibration was violent enough to break the hold of the epoxy on the frame and led to a crucial redesign.

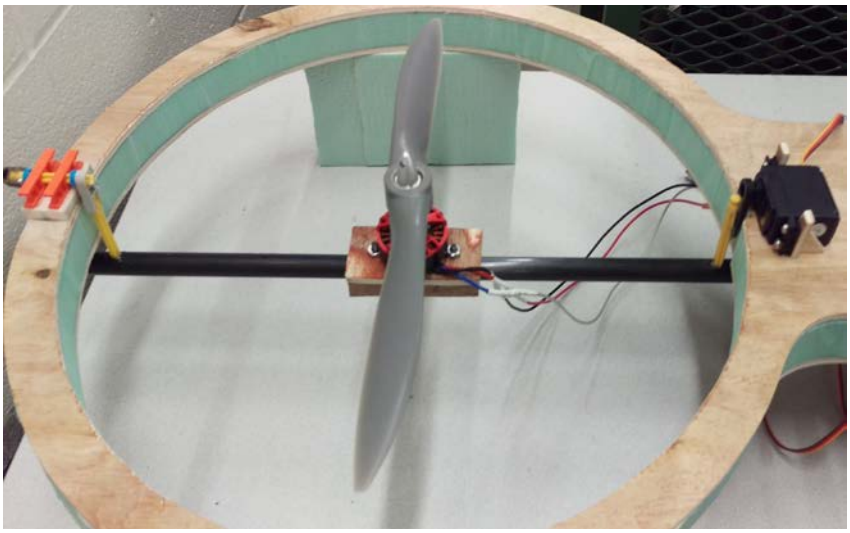

Figure 26: Initial servo/mounting spar configuration

The new configuration, shown in Figure 27, has the mounting spar fixed within rotational bearings that were directly mounted to the frame. Therefore, the motor and center of the propeller now rotate about the fixed spar. Consequently, when the motors tilt forward and backward for thrust vectoring, the center of the propeller rotates as well, bringing the propeller blades closer to the duct of the frame. However, at small enough angles, they do not come close enough to the duct of the frame for this to be a major concern. Mounting the spars directly to the frame nearly eliminated all vibrational issues experienced with the first configuration.

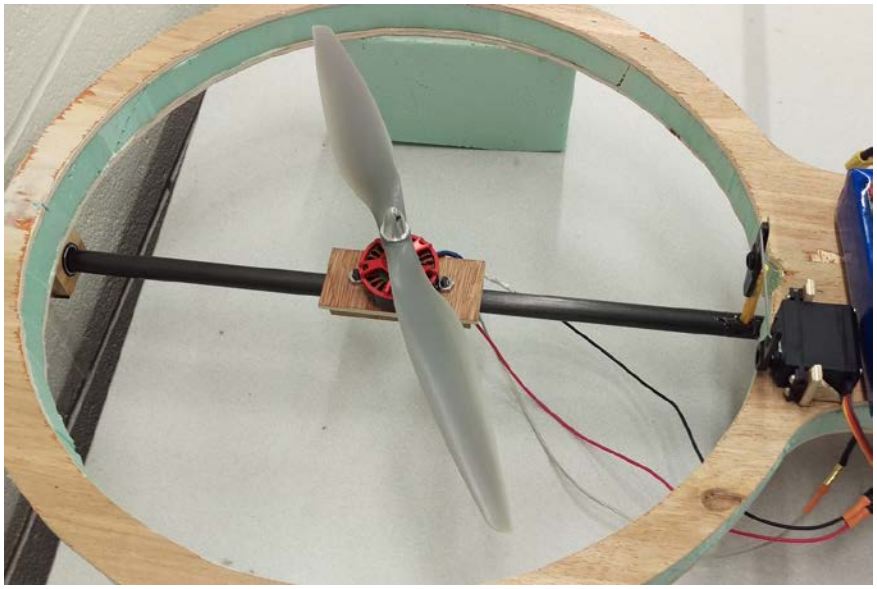

Figure 27: Modified servo/mounting spar configuration

Theoretically, the Y-splitter would have worked in creating synchronized signals to each of the motors and led to equal thrust and RPM from each propeller. Unfortunately, because the real world is not theoretical, this did not work perfectly and the design had to be done away with and replaced with individual thrust control. This, coupled with the redesigned spar and servo configuration, called for a new round of flight testing. This second round of testing confirmed the results from the simulation that were displayed in section 6. The basic outcome of the simulation and the flight testing was that the system is wildly unstable. Though there was a flight test where the thrusts were actually synchronized rather well, other tests showed that the smallest perturbation would lend to an uncontrollable roll divergence. Even the test with synchronized thrust had no measure of pitch control.

Figure 28: Example of rolling instability due to ground effect in testing

For the test shown above in Figure 28, the intent was to show what the result is of a small perturbation in the thrust of one of the rotors. The prototype was not free flying because of the knowledge of its inherent instability. Instead, it was attached to a carbon fiber rod that acted as a tethering device. This rod was attached along the body x-axis so as to allow for rolling rotation. Uneven thrust also produced a yawing moment, but that rotation was not seen in this flight test because of the tethering rod. Another test was conducted with the model tethered by fishing line. This test also illustrated yawing and pitching instabilities in the prototype. The benefit of this

second round of testing was that the outcomes of these tests confirmed the instabilities seen in the simulation. The prototype, as it is, does not have vibrational issues or signal lag due to different motors or wiring problems. This model is a physical representation of the model that was simulated. Both the simulation results and the flight tests show stability divergence due to perturbations.

8. Conclusion

As tandem rotor technology develops, the idea of manned “hover boards” becomes increasingly possible. One of the main obstacles in tandem rotor technology is controlling the vehicle while only having two coplanar rotors. As was found in this project, the rotational degrees of freedom are entirely unstable without additional control. This was shown in the dynamic simulation done in MATLAB and confirmed by the flight tests. In order for future tandem rotor hover boards to become a reality, there must be control to synchronize the rotors as well as some systems in place to counter the rotational instabilities. For addition means of control, swashplates could also be integrated into the design.

9. Future work

There is work that can be done in the future to both the physical prototype as well as the computer model of the system. If rate gyros are added to the system, a controller could know what the orientation angles of the system are. This controller could control the RPM of the rotors as well as the angular deflection of the servos to counter these angular motions caused by perturbations. Having this controller synchronize the rotor RPMs should help eliminate the need for more robust yaw and roll control. There would however still be a need for a more comprehensive pitch control method. As it stands, the system has no measure of pitch control, and synchronizing the rotors alone would not be able to remedy that problem. Longer term, accelerometers could also be added which would allow for a more autonomous flight system. If autonomous is not the direction desired, a friendlier user interface could be implemented.

10. References

[1] Lawler, M. A., Ivler, C. M., Tischler, M. B., Shtessel, Y. B. (2006). System Identification of the Longitudinal/Heave Dynamics for a Tandem-Rotor Helicopter Including Higher-Order Dynamics. *American Institute of Aeronautics and Astronautics.*

[2] *Ranstom Creations*. N.p., n.d. Web. <http://ranstomcreations.com/wp-content/uploads /2015/07/malloy-aeronautics-hoverbike-14.jpg>.

[3] M. F. Ashby: 'Materials Selection in Mechanical Design', fourth edition, 61, 67, 152-155, 252, 265-268, 531-533; 2011, Burlington, Elsevier Ltd.

[4] "Sandwich in Bending." *Boat Design*. N.p., n.d. Web. <http://www.boatdesign.net/assets/images/foam-core-1.gif>.

[5] Ross, Robert J. "Mechanical Properties of Wood-Based Composite Materials." *Wood Handbook*. By Zhiyong Cai. Madison, WI: Forest Products Laboratory, 2010. 2. Print.

[6] Nathan, N. D., Green, R. B. (2012). The flow around a model helicopter main rotor in ground effect. *Exp. Fluids, 52:*151-166.

[7] Staples, Gabriel. "Propeller Static & Dynamic Thrust Calculation." *Electric RC Aircraft Guy*. N.p., 16 July 2013. Web. May 2015

11. Appendices

11.1. Appendix A: Equation Derivation

Rotational Kinematics:

$$^{N}\underline{\omega}^{B} = {}^{N}\underline{\omega}^{N'} + {}^{N'}\underline{\omega}^{N''} + {}^{N''}\underline{\omega}^{B}$$

$$^{N}\underline{\omega}^{B} = \dot{\psi}\underline{N}' + \dot{\theta}\underline{N}'' + \dot{\phi}\underline{b}_1$$

$$^{N}\underline{\omega}^{B} = \dot{\psi}\left(-S_\theta \underline{N}_1'' + C_\theta \underline{N}_3''\right) + \dot{\theta}\left(C_\phi \underline{b}_2 - S_\phi \underline{b}_3\right) + \dot{\phi}\underline{b}_1$$

$$^{N}\underline{\omega}^{B} = \left(\dot{\phi} - \dot{\psi}S_\theta\right)\underline{b}_1 + \left(\dot{\theta}C_\phi + \dot{\psi}C_\theta S_\phi\right)\underline{b}_2 + \left(-\dot{\theta}S_\phi + \dot{\psi}C_\theta S_\phi\right)\underline{b}_3$$

$$\begin{bmatrix} p \\ q \\ r \end{bmatrix} = \begin{bmatrix} 1 & 0 & -S_\Phi \\ 0 & C_\Phi & S_\Phi C_\theta \\ 0 & -S_\Phi & C_\Phi C_\theta \end{bmatrix} \begin{bmatrix} \dot{\Phi} \\ \dot{\theta} \\ \dot{\psi} \end{bmatrix}$$

$$\dot{\Phi} = p + (sin\Phi tan\theta)q + (cos\Phi tan\theta)r$$

$$\dot{\theta} = (cos\Phi)q - (sin\Phi)r$$

$$\dot{\psi} = (sin\Phi sec\theta)q + (cos\Phi sec\theta)r$$

Translational Kinematics:

$$^{N}v_N^{B^*} = L_{NB}{}^{N}v_B^{B^*}$$

$$\begin{bmatrix} \dot{x}_e \\ \dot{y}_e \\ \dot{z}_e \end{bmatrix} = \begin{bmatrix} C_\theta C_\psi & S_\Phi S_\theta C_\psi - C_\Phi S_\psi & C_\Phi S_\theta C_\psi + S_\Phi S_\psi \\ C_\theta S_\psi & S_\Phi S_\theta S_\psi + C_\Phi C_\psi & C_\Phi S_\theta S_\psi - S_\Phi C_\psi \\ -S_\theta & S_\Phi C_\theta & C_\Phi C_\theta \end{bmatrix} \begin{bmatrix} u \\ v \\ w \end{bmatrix}$$

$$\dot{x}_e = \left(C_\theta C_\psi\right)u + \left(S_\Phi S_\theta C_\psi - C_\Phi S_\psi\right)v + \left(C_\Phi S_\theta C_\psi + S_\Phi S_\psi\right)w$$

$$\dot{y}_e = \left(C_\theta S_\psi\right)u + \left(S_\Phi S_\theta S_\psi + C_\Phi C_\psi\right)v + \left(C_\Phi S_\theta S_\psi - S_\Phi C_\psi\right)w$$

$$\dot{z}_e = (-S_\theta)u + (S_\Phi C_\theta)v + (C_\Phi C_\theta)w$$

Rotational Dynamics:

$$\underline{M}^{B^*} = {}^{N}\frac{d}{dt}\left({}^{N}\underline{H}^{B^*}\right) = {}^{B}\frac{d}{dt}\left({}^{N}\underline{H}^{B^*}\right) + \left({}^{N}\underline{\omega}^{B} \times {}^{N}\underline{H}^{B^*}\right)$$

$$\begin{bmatrix}\dot{p}\\ \dot{q}\\ \dot{r}\end{bmatrix} = -\begin{bmatrix}I_{xx} & 0 & 0\\ 0 & I_{yy} & 0\\ 0 & 0 & I_{zz}\end{bmatrix}^{-1}\begin{bmatrix}0 & -r & q\\ r & 0 & -p\\ -q & p & 0\end{bmatrix}\begin{bmatrix}I_{xx} & 0 & 0\\ 0 & I_{yy} & 0\\ 0 & 0 & I_{zz}\end{bmatrix}\begin{bmatrix}p\\ q\\ r\end{bmatrix} + \begin{bmatrix}I_{xx} & 0 & 0\\ 0 & I_{yy} & 0\\ 0 & 0 & I_{zz}\end{bmatrix}^{-1}\begin{bmatrix}L\\ M\\ N\end{bmatrix}$$

$$\begin{bmatrix}\dot{p}\\ \dot{q}\\ \dot{r}\end{bmatrix} = -[I]^{-1}\begin{bmatrix}0 & -r & q\\ r & 0 & -p\\ -q & p & 0\end{bmatrix}\begin{bmatrix}pI_{xx}\\ qI_{yy}\\ rI_{zz}\end{bmatrix} + \begin{bmatrix}L/I_{xx}\\ M/I_{yy}\\ N/I_{zz}\end{bmatrix}$$

$$\begin{bmatrix}\dot{p}\\ \dot{q}\\ \dot{r}\end{bmatrix} = -\begin{bmatrix}1/I_{xx} & 0 & 0\\ 0 & 1/I_{yy} & 0\\ 0 & 0 & 1/I_{zz}\end{bmatrix}\begin{bmatrix}-rqI_{yy} + qrI_{zz}\\ rpI_{xx} - prI_{zz}\\ -qpI_{xx} + pqI_{yy}\end{bmatrix} + \begin{bmatrix}L/I_{xx}\\ M/I_{yy}\\ N/I_{zz}\end{bmatrix}$$

$$\begin{bmatrix}\dot{p}\\ \dot{q}\\ \dot{r}\end{bmatrix} = \begin{bmatrix}qr\left(\frac{I_{yy}-I_{zz}}{I_{xx}}\right)\\ pr\left(\frac{I_{zz}-I_{xx}}{I_{yy}}\right)\\ pq\left(\frac{I_{xx}-I_{yy}}{I_{zz}}\right)\end{bmatrix} + \begin{bmatrix}L/I_{xx}\\ M/I_{yy}\\ N/I_{zz}\end{bmatrix}$$

$$\dot{p} = qr\frac{I_{yy}-I_{zz}}{I_{xx}} + \frac{L}{I_{xx}}$$

$$\dot{q} = pr\frac{I_{zz}-I_{xx}}{I_{yy}} + \frac{M}{I_{yy}}$$

$$\dot{r} = pq\frac{I_{xx}-I_{yy}}{I_{zz}} + \frac{N}{I_{zz}}$$

Translational Dynamics:

$$\sum \underline{F} = m^N \underline{\ddot{a}}^{B^*}$$

$${}^N\underline{a}^{B^*} = {}^N\frac{d}{dt}\left({}^N\underline{V}_B^{B^*}\right) = {}^B\frac{d}{dt}\left({}^N\underline{V}_B^{B^*}\right) + \left({}^N\underline{\omega}^B \times {}^N\underline{V}_B^{B^*}\right)$$

$${}^N\underline{a}^{B^*} = {}^N\underline{a}_B^{B^*} + {}^N\underline{\widetilde{\omega}}^B {}^N\underline{V}_B^{B^*}$$

$${}^N\underline{a}^{B^*} = \begin{bmatrix}\dot{u}\\ \dot{v}\\ \dot{w}\end{bmatrix} + \begin{bmatrix}0 & -r & q\\ r & 0 & -p\\ -q & p & 0\end{bmatrix}\begin{bmatrix}u\\ v\\ w\end{bmatrix}$$

$$\sum \underline{F} = \underline{T} + m\underline{g} + \underline{F}_{L/G}$$

$$\sum \underline{F} = \begin{bmatrix}T_x\\ T_y\\ T_z\end{bmatrix} + L_{BN}\begin{bmatrix}0\\ 0\\ mg\end{bmatrix} + 0$$

$$\begin{bmatrix}\dot{u}\\ \dot{v}\\ \dot{w}\end{bmatrix} = -\begin{bmatrix}0 & -r & q\\ r & 0 & -p\\ -q & p & 0\end{bmatrix}\begin{bmatrix}u\\ v\\ w\end{bmatrix} + \begin{bmatrix}T_x/m\\ T_y/m\\ T_z/m\end{bmatrix} + g\begin{bmatrix}-S_\theta\\ S_\phi C_\theta\\ C_\phi C_\theta\end{bmatrix}$$

$$\dot{u} = rv - qw - g(\sin\theta) + \frac{T_x}{m}$$

$$\dot{v} = pw - ru + g(sin\phi\ cos\theta) + \frac{T_y}{m}$$

$$\dot{w} = qu - rv + g(cos\phi\ cos\theta) + \frac{T_z}{m}$$

Linearization of Equations:

- *This is for the hovering flight case only*
- *The forward flight case is linearized similarly, except an initial velocity exists in the body x-axis*

$$\dot{u} = rv - gw - gS_\theta + \frac{1}{m}(T_x) \longrightarrow 0 = -gS_\theta + \frac{T_x}{m}$$

$$\dot{v} = pw - ru + gC_\theta S_\Phi + \frac{1}{m}(T_y) \longrightarrow 0 = gC_\theta S_\Phi$$

$$\dot{w} = qu - pv + gC_\theta C_\Phi + \frac{1}{m}(T_z) \longrightarrow 0 = gC_\theta C_\Phi + \frac{T_z}{m}$$

$$\dot{u_0} + \Delta\dot{u} = (r_0 + \Delta r)(v_0 + \Delta v) - (q_0 + \Delta q)(w_0 + \Delta w) - g * \sin(\theta_0 + \Delta\theta) + \frac{1}{m}(T_{x_0} + \Delta T_x)$$

$$\Delta\dot{u} = r_0 v_0 + \Delta r v_0 + r_0 \Delta v - q_0 w_0 + \Delta q w_0 + q_0 \Delta w - g\left(S_{\theta_0} + C_{\theta_0}\Delta\theta\right) + \frac{1}{m}(T_{x_0} + \Delta T_x)$$

$$\boxed{\Delta\dot{u} = -g\Delta\theta + \frac{1}{m}\Delta T_x}$$

$$\dot{v_0} + \Delta\dot{v} = (p_0 + \Delta p)(w_0 + \Delta w) - (r_0 + \Delta r)(u_0 + \Delta u) + g * \cos(\theta_0 + \Delta\theta) * \sin(\Phi_0 + \Delta\Phi) + \frac{1}{m}(T_{y_0} + \Delta T_y)$$

$$\Delta\dot{v} = p_0 w_0 + \Delta w p_0 + w_0 \Delta p - r_0 u_0 + \Delta u r_0 + u_0 \Delta r + g(cos\theta_0 - sin\theta_0\Delta\theta)(S_\Phi + C_\Phi\Delta\Phi) + \frac{1}{m}(T_{y_0} + \Delta T_y)$$

$$\boxed{\Delta\dot{v} = \frac{1}{m}\Delta T_y + g\Delta\Phi}$$

$$\dot{w_0} + \Delta\dot{w} = (q_0 + \Delta q)(u_0 + \Delta u) - (p_0 + \Delta p)(v_0 + \Delta v) + g * \cos(\theta_0 + \Delta\theta) * \cos(\Phi_0 + \Delta\Phi) + \frac{1}{m}(T_{z_0} + \Delta T_z)$$

$$\Delta\dot{w} = g(cos\theta_0 - sin\theta_0\Delta\theta)(cos\Phi_0 - sin\Phi_0\Delta\Phi) + \frac{1}{m}(T_{z_0} + \Delta T_z)$$

$$\Delta\dot{w} = g\left(C_{\theta_0}C_{\Phi_0} - C_{\theta_0}S_{\Phi_0}\Delta\Phi - C_{\Phi_0}S_{\theta_0}\Delta\theta\right) + \frac{1}{m}(T_{z_0} + \Delta T_z)$$

$$\boxed{\Delta\dot{w} = \frac{1}{m}\Delta T_z + g}$$

$$\dot{p} = qr\left(\frac{I_{yy} - I_{zz}}{I_{xx}}\right) + \frac{L}{I_{xx}}$$

$$\dot{p}_0 + \Delta\dot{p} = (q_0 + \Delta q)(r_0 + \Delta r)\left(\frac{I_{yy} - I_{zz}}{I_{xx}}\right) + \frac{L_0 + \Delta L}{I_{xx}}$$

$$\dot{p}_0 + \Delta\dot{p} = (q_0 r_0 + q_0\Delta r + r_0\Delta q + \Delta q\Delta r)\left(\frac{I_{yy} - I_{zz}}{I_{xx}}\right) + \frac{\Delta L}{I_{xx}}$$

$$\boxed{\Delta\dot{p} = \frac{\Delta L}{I_{xx}}}$$

$$\dot{q} = pr\left(\frac{I_{zz} - I_{xx}}{I_{yy}}\right) + \frac{M}{I_{yy}}$$

$$\dot{q}_0 + \Delta\dot{q} = (p_0 + \Delta p)(r_0 + \Delta r)\left(\frac{I_{zz} - I_{xx}}{I_{yy}}\right) + \frac{M_0 + \Delta M}{I_{yy}}$$

$$\boxed{\Delta\dot{q} = \frac{\Delta M}{I_{yy}}}$$

$$\dot{r} = pq\left(\frac{I_{xx} - I_{yy}}{I_{zz}}\right) + \frac{N}{I_{zz}}$$

$$\dot{r}_0 + \Delta\dot{r} = (p_0 + \Delta p)(q_0 + \Delta q)\left(\frac{I_{xx} - I_{yy}}{I_{zz}}\right) + \frac{N_0 + \Delta N}{I_{zz}}$$

$$\boxed{\Delta\dot{r} = \frac{\Delta N}{I_{zz}}}$$

$$\dot{x} = \left(C_\theta C_\psi\right)u + \left(S_\Phi S_\theta C_\psi - C_\Phi S_\psi\right)v + \left(C_\Phi S_\theta C_\psi + S_\Phi S_\psi\right)w$$

$$(\dot{x}_0 + \Delta\dot{x}) = \cos(\theta_0 + \Delta\theta)\cos(\psi_0 + \Delta\psi)\,(u_0 + \Delta u) + [\sin(\Phi_0 + \Delta\Phi)\sin(\theta_0 + \Delta\theta)\cos(\psi_0 + \Delta\psi) - \cos(\Phi_0 + \Delta\Phi) - \sin(\psi_0 + \Delta\psi)](v_0 + \Delta v) + [\cos(\Phi_0 + \Delta\Phi)\sin(\theta_0 + \Delta\theta)\cos(\psi_0 + \Delta\psi) + \sin(\Phi_0 + \Delta\Phi)\sin(\psi_0 + \Delta\psi)](w_0 + \Delta w)$$

$$\Delta\dot{x} = \big(C_{\theta_0}C_{\Delta\theta} - S_{\theta_0}S_{\Delta\theta}\big)\big(C_{\psi_0}C_{\Delta\psi} - S_{\psi_0}S_{\Delta\psi}\big)\Delta u + \big[\big(S_{\Phi_0}C_{\Delta\Phi} + C_{\Phi_0}S_{\Delta\Phi}\big)\big(S_{\theta_0}C_{\Delta\theta} + C_{\theta_0}S_{\Delta\theta}\big)\cos(\psi_0 + \Delta\psi) - \big(C_{\Phi_0}C_{\Delta\Phi} - S_{\Phi_0}S_{\Delta\Phi}\big)\big(S_{\psi_0}C_{\Delta\psi} + C_{\psi_0}S_{\Delta\psi}\big)\big]\Delta v + \big[\big(C_{\Phi_0}C_{\Delta\Phi} - S_{\Phi_0}S_{\Delta\Phi}\big)\big(S_{\theta_0}C_{\Delta\theta} + C_{\theta_0}S_{\Delta\theta}\big)\big(C_{\psi_0}C_{\Delta\psi} - S_{\psi_0}S_{\Delta\psi}\big) + \big(S_{\Phi_0}C_{\Delta\Phi} + C_{\Phi_0}S_{\Delta\Phi}\big)\big(S_{\psi_0}C_{\Delta\psi} + C_{\psi_0}S_{\Delta\psi}\big)\big]\Delta w$$

$$\Delta\dot{x} = \big(C_{\psi_0} - S_{\psi_0}\Delta\psi\big)\Delta u + \big(S_{\psi_0} + C_{\psi_0}\Delta\psi\big)\Delta v + \big[\Delta\theta\big(C_{\psi_0} - S_{\psi_0}\Delta\psi\big) + \Delta\Phi(S_{\psi_0} + C_{\psi_0}\Delta\psi)\big]\Delta w$$

$$\boxed{\Delta\dot{x} = (cos\psi_0)\Delta u + (sin\psi_0)\Delta v}$$

$$\dot{y} = \big(C_\theta S_\psi\big)u + \big(S_\Phi S_\theta S_\psi + C_\Phi C_\psi\big)v + \big(C_\Phi S_\theta S_\psi - S_\Phi C_\psi\big)w$$

$$\dot{y}_0 + \Delta\dot{y} = \cos(\theta_0 + \Delta\theta)\sin(\psi_0 + \Delta\psi)\,(u_0 + \Delta u) + [\sin(\Phi_0 + \Delta\Phi)\sin(\theta_0 + \Delta\theta)\sin(\psi_0 + \Delta\psi) + \cos(\Phi_0 + \Delta\Phi)\cos(\psi_0 + \Delta\psi)](v_0 + \Delta v) + [\cos(\Phi_0 + \Delta\Phi)\sin(\theta_0 + \Delta\theta)\sin(\psi_0 + \Delta\psi) - \cos(\Phi_0 + \Delta\Phi)](w_0 + \Delta w)$$

$$\dot{y}_0 + \Delta\dot{y} = \big(C_{\theta_0}C_{\Delta\theta} - S_{\theta_0}S_{\Delta\theta}\big)\big(S_{\psi_0}C_{\Delta\psi} + C_{\psi_0}S_{\Delta\psi}\big)\Delta u + \big[\big(S_{\Phi_0}C_{\Delta\Phi} + C_{\Phi_0}S_{\Delta\Phi}\big)\big(S_{\theta_0}C_{\Delta\theta} + C_{\theta_0}S_{\Delta\theta}\big)\sin(\psi_0 + \Delta\psi) + \big(C_{\Phi_0}C_{\Delta\Phi} - S_{\Phi_0}S_{\Delta\Phi}\big)\big(C_{\psi_0}C_{\Delta\psi} - S_{\psi_0}S_{\Delta\psi}\big)\big]\Delta v + \big[\big(C_{\Phi_0}C_{\Delta\Phi} - S_{\Phi_0}S_{\Delta\Phi}\big)\big(S_{\theta_0}C_{\Delta\theta} + C_{\theta_0}S_{\Delta\theta}\big)\sin(\psi_0 + \Delta\psi) - \Delta\Phi cos(\psi_0 + \Delta\psi)\big]\Delta w$$

$$\Delta\dot{y} = \big(S_{\psi_0} - C_{\psi_0}\Delta\psi\big)\Delta u + \big(C_{\psi_0} - S_{\psi_0}\Delta\psi\big)\Delta v + \big[\Delta\Phi\big(C_{\psi_0} - S_{\psi_0}\Delta\psi\big) + \Delta\Phi(C_{\psi_0} - S_{\psi_0}\Delta\psi)\big]\Delta w$$

$$\boxed{\Delta\dot{y} = (sin\psi_0)\Delta u + (cos\psi_0)\Delta v}$$

$$\dot{z} = -S_\theta u + (S_\Phi C_\theta)v + (C_\Phi C_\theta)w$$

$$\dot{z}_0 + \Delta\dot{z} = -\sin(\theta_0 + \Delta\theta)\,(u_0 + \Delta u) + \sin(\Phi_0 + \Delta\Phi)\cos(\theta_0 + \Delta\theta)\,(v_0 + \Delta v) + \cos(\Phi_0 + \Delta\Phi)\cos(\theta_0 + \Delta\theta)\,(w_0 + \Delta w)$$

$$\Delta\dot{z} = \Delta\theta\Delta u + \Delta\Phi\Delta v + \Delta w$$

$$\boxed{\Delta\dot{z} = \Delta w}$$

$$\dot{\Phi} = p + (sin\Phi tan\theta)q + (cos\Phi tan\theta)r$$

$$\dot{\Phi}_0 + \Delta\dot{\Phi} = (p_0 + \Delta p) + \sin(\Phi_0 + \Delta\Phi)\tan(\theta_0 + \Delta\theta)(q_0 + \Delta q) + \cos(\Phi_0 + \Delta\Phi)\tan(\theta_0 + \Delta\theta)(r_0 + \Delta r)$$

$$\Delta\dot{\Phi} = \Delta p + \left(S_{\Phi_0}C_{\Delta\Phi} + C_{\Phi_0}S_{\Delta\Phi}\right)\left(\frac{T_{\theta_0} + T_{\Delta\theta}}{1 - T_{\theta_0}T_{\Delta\theta}}\right)\Delta q + \left(C_{\Phi_0}C_{\Delta\Phi} - S_{\Phi_0}S_{\Delta\Phi}\right)\left(\frac{T_{\theta_0} + T_{\Delta\theta}}{1 - T_{\theta_0}T_{\Delta\theta}}\right)\Delta r$$

$$\Delta\dot{\Phi} = \Delta p + \Delta\Phi\Delta\theta\Delta q + \Delta\theta\Delta r$$

$$\boxed{\Delta\dot{\Phi} = \Delta p}$$

$$\dot{\theta} = (cos\Phi)r - (sin\Phi)r$$

$$\dot{\theta}_0 + \Delta\dot{\theta} = \cos(\Phi_0 + \Delta\Phi)(q_0 + \Delta q) - \sin(\Phi_0 + \Delta\Phi)(r_o + \Delta r)$$

$$\Delta\dot{\theta} = \Delta q - \Delta\Phi\Delta r$$

$$\boxed{\Delta\dot{\theta} = \Delta q}$$

$$\dot{\psi} = (sin\Phi sec\theta)q + (cos\Phi sec\theta)r$$

$$\dot{\psi}_0 + \Delta\dot{\psi} = \sin(\Phi_0 + \Delta\Phi)\sec(\theta_0 + \Delta\theta)(q_0 + \Delta q) + \cos(\Phi_0 + \Delta\Phi)\sec(\theta_0 + \Delta\theta)(r_0 + \Delta r)$$

$$where \quad \sec(\theta_0 + \Delta\theta) = \frac{1}{\cos(\theta_0 + \Delta\theta)} = \frac{1}{C_{\theta_0}C_{\Delta\theta} - S_{\theta_0}S_{\Delta\theta}} = \frac{1}{1}$$

$$\Delta\dot{\psi} = (\Delta\Phi)(1)(\Delta q) + (1)(1)(\Delta r)$$

$$\boxed{\Delta\dot{\psi} = \Delta r}$$

11.2. Appendix B: Thrust Curve MATLAB Code

```
%% Thrust vs. RPM Curve

%{
    This code is broken into two sections. The first outputs a single
    thrust value based on the inputs of RPM, propeller diameter and
    propeller pitch. The second plots a thrust curve based on the diameter
    and pitch specified, plotting the thrust in pounds of the propeller vs
    the RPM for the range specified.
%}

close all;
clear;
clc;

RPM     = 11470;    % RPM
d       = 14;       % Diameter, inches
p       = 6;        % Pitch, inches

% Equation to calculate thrust
% Source:    http://www.electricrcaircraftguy.com/2013/09/propeller-static-
%            dynamic-thrust-equation.html#.VYS4VPlViko
F  = (1.225*pi/4*(.0254*d)^2*((RPM*.0254*p/60)^2)* ...
     (d/(3.29546*p))^1.5)*.224809;

% Simplified form
F  = (1.330601749098882e-12)*pi*RPM^2*d^2*p^2*(d/p)^(3/2);

%% Thrust v RPM curve

d       = 14;
p       = 6;
RPM     = 0:100:11500;

for i   = 1:length(RPM);
    F(i)  =  (1.330601749098882e-12)*pi*RPM(i)^2*d^2*p^2*(d/p)^(3/2);
end

figure(1)
plot(RPM,F); grid on;
xlabel('RPM')
ylabel('Thrust [pounds]')
title('Constant: Diameter, Pitch')
```

11.3. Appendix C: Ideal Hovering MATLAB Code

```
%% Ideal Flight Simulation

%{
    This code simululates the ideal motion of the tandem rotor hovering
    vehicle when subjected to various control inputs. The equations of
    motion were derived from basic principles, and then linearized about an
    equilibrium position; in this case, hovering flight. Therfore, a linear
    simulation operator is used to obtain the outputs of the system with
    various given inputs.

    The inputs of interest include both a step & doublet input for the
    forward motion case, as well as the turning motion case. These results
    are analyzed in the "Modeling and Simulation" section of the report.
%}

close all;
clear;
clc;

d2r     =  pi/180;       % degrees to radians conversion
r2d     =  180/pi;       % radians to degrees conversion
g       =  32.2;         % acceleration due to gravity, ft/s^2
m       =  3.89/g;       % mass, slugs
Ix      =  39.35/g;      % mass moment of inertia about x, slugs*in^2
Iy      =  366.08/g;     % mass moment of inertia about y, slugs*in^2
Iz      =  399.45/g;     % mass moment of inertia about z, slugs*in^2
T       =  m*g;          % thrust, slug*ft/s^2
zd      =  17;           % moment arm from rotor to CG, in
psi0    =  0;            % initial yaw angle

% Creation of the state space elements
A       =  zeros(12);
A(1,11)  =  -g;
A(2,10)  =  g;
A(7,1)   =  cos(psi0);
A(7,2)   =  -sin(psi0);
A(8,1)   =  sin(psi0);
A(8,2)   =  cos(psi0);
A(9,3)   =  1;
A(10,4)  =  1;
A(11,5)  =  1;
A(12,6)  =  1;

B       =  zeros(12,3);
B(1,:)   =  [T/m T/m 0];
B(3,:)   =  [0 0 T/m];
B(4,:)   =  [0 T*zd/Ix -T*zd/Ix];
B(6,:)   =  [T*zd/Iz -T*zd/Iz 0];

C       =  eye(12);

D       =  0;
```

```
sys      =  ss(A,B,C,D);
x0       =  zeros(1,12);

%% Forward step

tf      =  3;
dt      =  .01;
tspan   =  0:dt:tf;
del     =  5*d2r;       % radian servos input

U                   =  zeros(length(tspan),3);
U(1:1/dt,1:2)       =  sin(0);
U(1:1/dt,3)         =  cos(0);
U(1.01/dt:end,1:2)  =  sin(del);
U(1.01/dt:end,3)    =  cos(del);

FS  =  lsim(sys,U,tspan,x0);

figure(1)
subplot(311)
plot(tspan,FS(:,1)); title('X-body velocity'); ylabel('[in/s]')
subplot(312)
plot(tspan,FS(:,7)); title('Inertial X position'); ylabel('[in]')
subplot(313)
plot(tspan,FS(:,12)); title('Yaw angle'); ylabel('[rad]'); xlabel('time [s]')

%% Forward Doublet

U                     =  zeros(length(tspan),3);
U(1:1/dt,1:2)         =  sin(0);
U(1:1/dt,3)           =  cos(0);
U(1.01/dt:1.5/dt,1:2) =  sin(del);
U(1.01/dt:1.5/dt,3)   =  cos(del);
U(1.51/dt:2/dt,1:2)   =  -sin(del);
U(1.51/dt:2/dt,3)     =  cos(del);
U(2.01/dt:end,1:2)    =  sin(0);
U(2.01/dt:end,3)      =  cos(0);

FD  =  lsim(sys,U,tspan,x0);

figure(2)
subplot(311)
plot(tspan,FD(:,1)); title('X-body velocity'); ylabel('[in/s]')
subplot(312)
plot(tspan,FD(:,7)); title('Inertial X position'); ylabel('[in]')
subplot(313)
plot(tspan,FD(:,12)); title('Yaw angle'); ylabel('[rad]'); xlabel('time [s]')


%% Turning Step
U                =  zeros(length(tspan),3);
U(1:1/dt,1:2)    =  sin(0);
U(1:1/dt,3)      =  cos(0);
```

```
U(1.01/dt:end,1)  =  -sin(del);
U(1.01/dt:end,2)  =  sin(del);
U(1.01/dt:end,3)  =  cos(del);

TS  =  lsim(sys,U,tspan,x0);

figure(3)
subplot(311)
plot(tspan,TS(:,6)); title('Yaw rate'); ylabel('[rad/s]')
subplot(312)
plot(tspan,TS(:,7)); title('Inertial X position'); ylabel('[in]')
subplot(313)
plot(tspan,TS(:,12)); title('Yaw angle'); ylabel('[rad]'); xlabel('time [s]')


%% Turning Doublet
U                    =  zeros(length(tspan),3);
U(1:1/dt,1:2)        =  sin(0);
U(1:1/dt,3)          =  cos(0);
U(1.01/dt:1.5/dt,1)  =  -sin(del);
U(1.01/dt:1.5/dt,2)  =  sin(del);
U(1.01/dt:1.5/dt,3)  =  cos(del);
U(1.51/dt:2/dt,1)    =  sin(del);
U(1.51/dt:2/dt,2)    =  -sin(del);
U(1.51/dt:2/dt,3)    =  cos(del);
U(2.01/dt:end,1:2)   =  sin(0);
U(2.01/dt:end,3)     =  cos(0);

TD  =  lsim(sys,U,tspan,x0);

figure(4)
subplot(311)
plot(tspan,TD(:,6)); title('Yaw rate'); ylabel('[rad/s]')
subplot(312)
plot(tspan,TD(:,7)); title('Inertial X position'); ylabel('[in]')
subplot(313)
plot(tspan,TD(:,12)); title('Yaw angle'); ylabel('[rad]'); xlabel('time [s]')
```

11.4. Appendix D: Non-Ideal Hovering MATLAB Code

```
%% Hovering Flight Simulation

%{
    This code simulates the motion of the tandem rotor hovering vehicle
    when subjected to various control inputs. The equations of motion were
    derived from basic principles, and then linearized about an equilibrium
    position; in this case, hovering flight. Therfore, a linear simulation
    operator is used to obtain the outputs of the system with various
    given inputs.

    The inputs of interest include impulse perturbations of thrust on one
    propeller and deflection of one servo. These results are analyzed in
    the "Modeling and Simulation" section of the report.
%}

close all
clear
clc

d2r     = pi/180;       % degrees to radians conversion
r2d     = 180/pi;       % radians to degrees conversion
g       = 32.2;         % acceleration due to gravity, ft/s^2
m       = 3.89/g;       % mass, slugs
Ix      = 39.35/g;      % mass moment of inertia about x, slugs*in^2
Iy      = 366.08/g;     % mass moment of inertia about y, slugs*in^2
Iz      = 399.45/g;     % mass moment of inertia about z, slugs*in^2
T1      = 0.5*m*g/12;   % thrust, slug*in/s^2
T2      = 0.5*m*g/12;   % thrust, slug*in/s^2
k       = 1;            % assume ideal situation
RPM1    = (T1/((1.330601749098882e-12)*pi*14^2*5.5^2*(14/5.5)^(3/2))).^0.5;
RPM2    = (T2/((1.330601749098882e-12)*pi*14^2*5.5^2*(14/5.5)^(3/2))).^0.5;
Torque1 = 5.5*14^4*RPM1.^2*5.33*10E-15*5252*k/74/144;   % slugs*in^2*s^-2
Torque2 = 5.5*14^4*RPM2.^2*5.33*10E-15*5252*k/74/144;   % slugs*in^2*s^-2
zd      = 17;           % moment arm from rotor to CG, in
psi0    = 0;            % initial yaw angle

% Creation of the state space elements
A       =  zeros(12);
A(1,11)  =  -g;
A(2,10)  =  g;
A(7,1)   =  cos(psi0);
A(7,2)   =  -sin(psi0);
A(8,1)   =  sin(psi0);
A(8,2)   =  cos(psi0);
A(9,3)   =  1;
A(10,4)  =  1;
A(11,5)  =  1;
A(12,6)  =  1;

B       =  zeros(12,4);
B(1,:)  =  [1 1 0 0];
B(3,:)  =  [0 0 1 1];
```

```
B(4,:)  =  [0 0 zd/Ix -zd/Ix];
B(6,:)  =  [zd/Iz -zd/Iz (Torque1/T1)/Iz -(Torque2/T2)/Iz];

C       =  eye(12);

D       =  0;

sys     =  ss(A,B,C,D);

x0      =  zeros(1,12);


%% Uneven thrust perturbation

tf     =  3;
dt     =  .01;
tspan  =  0:dt:tf;
del    =  5*d2r;

U                 =  zeros(length(tspan),4);
U(1:end,1:2)      =  0*sin(0);
U(1:end,3:4)      =  0*cos(0);
U(1/dt:1.1/dt,3)  =  cos(0);


UTP  =  lsim(sys,U,tspan,x0);

figure(1)
subplot(411)
plot(tspan,UTP(:,10)); title('Roll angle'); ylabel('[rad]'),grid
subplot(412)
plot(tspan,UTP(:,8)); title('Inertial Y position'); ylabel('[in]'),grid
subplot(413)
plot(tspan,UTP(:,2)); title('Y-body velocity'); ylabel('[in/s]'),grid
subplot(414)
plot(tspan,UTP(:,12)); title('Yaw angle'); ylabel('[rad]')
xlabel('time [s]'), grid


%% Uneven servo deflection perturbation

U                 =  zeros(length(tspan),4);
U(1:end,1:2)      =  0*sin(0);
U(1:end,3:4)      =  0*cos(0);
U(1/dt:1.1/dt,1)  =  sin(del);
U(1/dt:1.1/dt,3)  =  cos(del)-1;


USP  =  lsim(sys,U,tspan,x0);

figure(2)
subplot(411)
plot(tspan,USP(:,10)); title('Roll angle'); ylabel('[rad]'),grid
```

```
subplot(412)
plot(tspan,USP(:,8)); title('Inertial Y position'); ylabel('[in]'),grid
subplot(413)
plot(tspan,USP(:,7)); title('Inertial X position'); ylabel('[in]'),grid
subplot(414)
plot(tspan,USP(:,12)); grid on
title('Yaw angle'); ylabel('[rad]'); xlabel('time [s]')
```

11.5. Appendix E: Non-Ideal Forward Flight MATLAB Code

```
%% Forward Flight Simulation

%{
    This code simulates the motion of the tandem rotor hovering vehicle
    when subjected to different inputs. The equations of motion were
    derived from basic principles, and then linearized about an equilibrium
    position; in this case, forward flight with constant velocity. A linear
    simulation operated was used to obtain the outputs of the system with
    various given inputs.

    The inputs of interest include impulse perturbations of thrust on one
    propeller and deflection of one servo. These results are analyzed in
    the "Modeling and Simulation" section of the report.

%}

close all;
clear;
clc;

d2r     = pi/180;       % degrees to radians conversion
r2d     = 180/pi;       % radians to degrees conversion
g       = 32.2;         % acceleration due to gravity, ft/s^2
m       = 3.89/g;       % mass, slugs
Ix      = 39.35/g;      % mass moment of inertia about x, slugs*in^2
Iy      = 366.08/g;     % mass moment of inertia about y, slugs*in^2
Iz      = 399.45/g;     % mass moment of inertia about z, slugs*in^2
T1      = 0.5*m*g/12;   % thrust, slug*in/s^2
T2      = 0.5*m*g/12;   % thrust, slug*in/s^2
k       = 1;            % assume ideal condition
RPM1    = (T1/((1.330601749098882e-12)*pi*14^2*5.5^2*(14/5.5)^(3/2))).^0.5;
RPM2    = (T2/((1.330601749098882e-12)*pi*14^2*5.5^2*(14/5.5)^(3/2))).^0.5;
Torque1 = 5.5*14^4*RPM1.^2*5.33*10E-15*5252*k/74/144;   % slugs*in^2*s^-2
Torque2 = 5.5*14^4*RPM2.^2*5.33*10E-15*5252*k/74/144;   % slugs*in^2*s^-2
zd      = 17;           % moment arm from rotor to CG, in
psi0    = 0;            % initial yaw angle
u0      = 1;            % initial body-x velocity, in/s

% Creation of the State Space Elements
A        =  zeros(12);
A(1,11)  =  -g;
A(2,6)   =  -u0;
A(2,10)  =  g;
A(3,5)   =  u0;
A(7,1)   =  cos(psi0);
A(7,2)   =  -sin(psi0);
A(7,12)  =  -sin(psi0)*u0;
A(8,1)   =  sin(psi0);
A(8,2)   =  cos(psi0);
A(8,12)  =  cos(psi0)*u0;
A(9,3)   =  1;
A(9,11)  =  -u0;
```

```
A(10,4)  =  1;
A(11,5)  =  1;
A(12,6)  =  1;

B       =  zeros(12,4);
B(1,:)  =  [1 1 0 0];
B(3,:)  =  [0 0 1 1];
B(4,:)  =  [0 0 zd/Ix -zd/Ix];
B(6,:)  =  [zd/Iz -zd/Iz (Torque1/T1)/Iz -(Torque2/T2)/Iz];

C       =  eye(12);

D       =  0;

sys     =  ss(A,B,C,D);
x0      =  zeros(1,12);

% Constant velocity in the body-X direction
x0(1)   =  u0;


%% Uneven thrust perturbation

tf      =  3;
dt      =  .01;
tspan   =  0:dt:tf;
del     =  5*d2r;       % radian servos input

U                 =  zeros(length(tspan),4);
U(1:end,1:2)      =  0*sin(0);
U(1:end,3:4)      =  0*cos(0);
U(1/dt:1.1/dt,3)  =  cos(0);


FD  =  lsim(sys,U,tspan,x0);

figure(1)
subplot(411)
plot(tspan,FD(:,10)); title('Roll angle'); ylabel('[rad]'),grid
subplot(412)
plot(tspan,FD(:,8)); title('Inertial Y position'); ylabel('[in]'),grid
subplot(413)
plot(tspan,FD(:,2)); title('Y-body velocity'); ylabel('[in/s]'),grid
subplot(414)
plot(tspan,FD(:,12)); title('Yaw angle'); ylabel('[rad]')
xlabel('time [s]'),grid


%% Uneven servo deflection perturbation

U                 =  zeros(length(tspan),4);
U(1:end,1:2)      =  0*sin(0);
U(1:end,3:4)      =  0*cos(0);
U(1/dt:1.1/dt,1)  =  sin(del);
```

```
U(1/dt:1.1/dt,3)  =  cos(del)-1;


TS  =  lsim(sys,U,tspan,x0);

figure(2)
subplot(411)
plot(tspan,TS(:,10)); title('Roll angle'); ylabel('[rad]'),grid
subplot(412)
plot(tspan,TS(:,8)); title('Inertial Y position'); ylabel('[in]'),grid
subplot(413)
plot(tspan,TS(:,7)); title('Inertial X position'); ylabel('[in]'),grid
subplot(414)
plot(tspan,TS(:,12)); title('Yaw angle'); ylabel('[rad]')
xlabel('time [s]'),grid
```

11.6. Appendix F: Assessment of Student Outcomes

Assessment of Program Outcome #5
ME 4800

The MAE faculty members have identified "**An ability to design a system, component, or process to meet desired needs within realistic constraints such as economic, environmental, social, political, ethical, health and safety, manufacturability, and sustainability**" as one of the student outcomes for both mechanical and aeronautical engineering programs. As part of your design project, we ask you to answer the following questions. You are required to submit the completed form with your final report in ME 4800. In your final report, please include page references in response to each question below.

Evaluation of program outcome "**An ability to design a system, component, or process to meet desired needs within realistic constraints such as economic, environmental, social, political, ethical, health and safety, manufacturability, and sustainability**"

1. This project involved the design of a: ***system / component / process***

   Description:

   This project involved designing a tandem rotor vehicle which included the design and integration of various components of the flight system. (Pg. 7)

2. The ***need:***

   This study was motivated by the desire to further research in the field of modern rotocopter design and implementation. (Pg.5)

3. The **constraints:** (Explain and justify any constraint that was relevant to the project. At least 3 constraints must be addressed.)

   Economic:

   Initial limited funding of this project lead to design constraints because only inexpensive components and materials were used. (Pg. 7)

   Environmental:

   N/A

Social:

N/A

Political:

N/A

Ethical:

N/A

Health & Safety:

Our personal safety was a constraint during flight testing, which is why a tether was used on the vehicle. (Pg. 47)

Manufacturability:

This project had to be easily manufacturable due to our limited resources as students. An example would be making the frame out of three solid pieces for ease of build. (Pg. 8)

Sustainability:

N/A

Others:

N/A

4. Is there a potential for a new patent in your design? Explain and compare with related patents.

   Although other designs and patents are out there for tandem rotor vehicles, this project's vehicle is unique in its orientation and the design for controls, which may be patentable. (Pg. 5)

Assessment of Program Outcome #9
ME 4800

The MAE faculty members have identified "**A knowledge of contemporary issues**" as one of the student outcomes for both mechanical and aeronautical engineering programs. **Contemporary issues are any issues that you hear on the news related to new and old products and their safety, new innovations, technologies, standards, and regulations in general.** As you develop your proposal for your senior design project, we ask you to start answering the following questions. These questions would guide you in the development of ideas you need to include in your proposal and final project reports. You are required to submit the completed form with your final proposal in ME 4790 and again with your final report in ME 4800. In your proposal and report, please include page references in response to each question below.

Evaluation of program outcome "**A knowledge of contemporary issues**"

1. Why is this project needed now?

   The market for rotocopter vehicles is rapidly expanding, therefore, now is the time to introduce new designs into the market. (Pg. 5)

2. Describe any new technologies and recent innovations utilized to complete this project

   Human-piloted "hover boards" are a very new innovation and were used as a basis for this project. (Pg. 5)

3. If this project is done for a company-how will it expand their potential markets?

   N/A

4. How did you address any safety and/or legal issues pertaining to this project (e.g., OSHA, EPA, Human Factors, etc.)

   The only safety concern addressed was our personal safety and the safety of others around us during flight testing. This was controlled by tethering the vehicle during operation. (Pg. 47)

5. Are there any new standards or regulations on the horizon that could impact the development of this project?

   FAA standards could impact this project if it were developed into a full-scale model.

6. Is there a potential for a new patent in your design? Please document related patents.

   This vehicle is unique in its orientation, but this orientation is addressed in patent US20070034738A1.

Does this project impact:

Human Health?

- *No impact. (Full scale model may generate emissions)*

Wildlife?

- *No impact.*

Vegetation?

- *No impact.*

Does this project improve:

Human Interaction?

- *As a recreational vehicle, this project could provide a means for positive human interaction.*

Well being?

- *Again, as a recreational vehicle, this project may improve an individual's happiness.*

Safety?

- *This project does not improve safety.*

Others?

- *N/A*

Assessment of Program Outcome #13
ME 47800

The MAE faculty have identified "**A recognition of the need for, and ability to engage in life-long learning**" as one of the program outcomes for both mechanical and aeronautical engineering programs. As you develop your senior design project, we ask you to start answering the following questions. These questions will guide you tin the development of ideas you need to include in your final project report. You are required to submit the completed form in the last appendix of your final report. Please include the page numbers of the report that addresses the answers to the following questions.

Your responses will be used in the Evaluation of program outcome "**A recognition of the need for, and ability to engage in life-long learning.**"

A well-organized team brings necessary backgrounds and talents together that are needed to successfully execute the design process. Each team member plays an important role on the design team. Individual members must be prepared to gain any additional skills necessary, and improve existing skills during project execution. Your response to the questions below will be evaluated for our ability to convey the need for lifelong learning and your ability to be creative in recognizing the need and acquiring the requisite knowledge.

ME 4800
Mechanical and Aeronautical Engineering Design Project

For each team member:

1. List the skills you needed to execute your responsibilities on the project as outlined in ME 4790.
    - *Steve Beuerle: In charge of control systems. Needs understanding of tandem rotor dynamics and controls.*
    - *Brent Kostich: In charge of dynamic analysis. Needs understanding of relevant dynamics/control systems and the equations of motion.*
    - *Nicole St.Louis: In charge of structure/CAD. Needs understanding of structural loads and the ability to model in CAD.*
    - *Andrew Verstraete: In charge of propulsion and system integration. Needs understanding of aero propulsion and system design.*

2. List how you gained the requisite skill, or enhanced your existing skill, to the benefit of your design team and the project.
    - *Steve Beuerle: has taken ME 3600, ME 5550, and ME 5950*
    - *Brent Kostich: has taken ME 3600, ME 5550, and ME 5950*
    - *Nicole St.Louis: has taken ME 2560, IME 1420, and AE 4630*
    - *Andrew Verstraete: has taken AE 3800, ME 3350, ME 3600, AE 4660, and AE 4690*